Mechanochemical coupling of lipid organization and protein function through membrane thickness deformations

Ahis Shrestha, Osman Kahraman,* and Christoph A. Haselwandter

Department of Physics and Astronomy and Department of Quantitative and Computational Biology, University of Southern California, Los Angeles, California 90089, USA

(Received 19 November 2021; accepted 6 May 2022; published 25 May 2022)

Cell membranes are composed of a great variety of protein and lipid species with distinct unperturbed hydrophobic thicknesses. To achieve hydrophobic matching, the lipid bilayer tends to deform around membrane proteins so as to match the protein hydrophobic thickness at bilayer-protein interfaces. Such protein-induced distortions of the lipid bilayer hydrophobic thickness incur a substantial energy cost that depends critically on the bilayer-protein hydrophobic mismatch, while distinct conformational states of membrane proteins often show distinct hydrophobic thicknesses. As a result, hydrophobic interactions between membrane proteins and lipids can yield a rich interplay of lipid-protein organization and transitions in protein conformational state. We combine here the membrane elasticity theory of protein-induced lipid bilayer thickness deformations with the Landau-Ginzburg theory of lipid domain formation to systematically explore the coupling between local lipid organization, lipid and protein hydrophobic thickness, and protein-induced lipid bilayer thickness deformations in membranes with heterogeneous lipid composition. We allow for a purely mechanical coupling of lipid and protein composition through the energetics of protein-induced lipid bilayer thickness deformations as well as a chemical coupling driven by preferential interactions between particular lipid and protein species. We find that the resulting lipid-protein organization can endow membrane proteins with diverse and controlled mechanical environments that, via protein-induced lipid bilayer thickness deformations, can strongly influence protein function. The theoretical approach employed here provides a general framework for the quantitative prediction of how membrane thickness deformations influence the joint organization and function of lipids and proteins in cell membranes.

DOI: 10.1103/PhysRevE.105.054410

I. INTRODUCTION

Lipids and membrane proteins in cell membranes show an intricate, submicron organization into membrane domains that vary in molecular composition and hydrophobic thickness [1–4]. The resulting heterogeneity in the mechanical and chemical properties of cell membranes permits the local regulation of membrane protein function through lipid-protein interactions and plays a critical role in a variety of cellular processes [2–5]. Experiments suggest that cell membrane organization is influenced by preferential chemical interactions between particular lipid and protein species as well as nonspecific hydrophobic lipid-protein interactions [1–8]. For instance, some ion channels are thought to aggregate specific lipid species in their vicinity, thereby creating a local bilayer environment with controlled mechanical properties [9–11]. The resulting membrane domains may serve to bias ion channels towards closed or open conformational states, and hence modulate ion channel function.

The preferred hydrophobic thickness of lipid bilayers depends strongly on the lipid chain length [1–3,12], with a variation in bilayer hydrophobic thickness between roughly 3.4 nm and 4.4 nm for the lipid chain lengths typically found in cell membranes. Similarly, the hydrophobic thickness of membrane proteins varies substantially between different membrane proteins, and even among distinct conformational states of the same membrane protein. For instance, the closed and open conformational states of the mechanosensitive channel of large conductance (MscL) have approximate hydrophobic thicknesses of 3.8 nm and 2.6 nm [13,14], respectively. Differences in the preferred hydrophobic thickness of lipids and membrane proteins generally result in deformations of the lipid bilayer thickness in the vicinity of membrane proteins so as to achieve hydrophobic matching at bilayer-protein interfaces [15–18]. Such protein-induced lipid bilayer thickness deformations tend to incur a substantial energy cost $>10\ k_BT$ [15–18]. Protein-induced lipid bilayer thickness deformations yield, on the one hand, a coupling between protein conformational state and lipid bilayer thickness [15,19–23]. On the other hand, protein-induced lipid bilayer thickness deformations give rise to bilayer-mediated interactions between membrane proteins [16,24–28]. Such bilayer-thickness-mediated protein interactions tend to be strongly favorable at close enough separations for proteins with identical hydrophobic thickness, and can yield self-assembly of membrane protein clusters [29–36].

The energy cost of protein-induced lipid bilayer thickness deformations depends critically on the lipid chain length [15–18,37]. In membranes containing lipids with

*Present address: Udemy Inc., Istanbul, Turkey.

distinct chain lengths, one therefore expects a coupling between local lipid composition and membrane protein hydrophobic thickness. Expanding on a previous short communication [38], we systematically explore here the mechanochemical coupling of local lipid organization, protein and lipid hydrophobic thickness, and protein-induced lipid bilayer thickness deformations in bilayers with heterogeneous hydrophobic thickness. Our approach builds on previous work on lipid phase separation in bilayers with heterogeneous hydrophobic thickness [39,40], and on the coupling between bilayer mean curvature and lipid composition [41–43]. We describe how lipid-protein organization in bilayers with heterogeneous hydrophobic thickness can be captured quantitatively by combining the elasticity theory of lipid bilayer thickness deformations [15–17,24–28,44] with the Landau-Ginzburg (LG) theory of lipid domain formation [41,45–53]. We illustrate our theoretical approach for MscL, which provides a paradigm for the coupling of local lipid composition and membrane protein function [9,21,22,54]. In agreement with a wide range of experimental studies [1–3,55–57], we find that membrane hydrophobic thickness provides a key control parameter for lipid-protein organization and regulation in membranes with heterogeneous lipid composition.

This article is organized as follows. Section II develops the general theory of protein-induced lipid bilayer thickness deformations in bilayers with heterogeneous hydrophobic thickness. On the one hand, we thereby consider a purely mechanical, nonspecific coupling of lipid and protein composition through the energetics of protein-induced lipid bilayer thickness deformations [38]. On the other hand, we allow for a chemical coupling between the local lipid and protein compositions driven by preferential interactions between particular lipid and protein species [58–65]. Section III considers the most straightforward scenario of a single-membrane protein in a heterogeneous lipid bilayer composed of two lipid species with distinct lipid chain lengths. We determine how the local lipid composition around the membrane protein depends on the protein hydrophobic thickness, the lipid-protein chemical affinity, and the local lipid chemical potential. Using MscL as a model system, we show that lipid heterogeneity can induce transitions in the protein conformational state. In Sec. IV we consider the crowded membrane protein environments typical for cell membranes [1–5,18]. We find that heterogeneity in the lipid composition can expand the repertoire and range of bilayer-thickness-mediated protein interactions, can yield colocalization of lipids and membrane proteins according to their preferred hydrophobic thickness, and can strongly affect bilayer-mediated protein cooperativity in cell membranes. Section V provides a summary and discussion of our results.

II. PROTEIN-INDUCED MEMBRANE THICKNESS DEFORMATIONS IN HETEROGENEOUS LIPID BILAYERS

We aim here to explore generic features of the interplay between lipid-protein organization and membrane thickness deformations that are independent of most molecular details [38]. We therefore consider an idealized bilayer-protein system, in which a cylindrical membrane protein of radius R is located at the center of a circular membrane patch

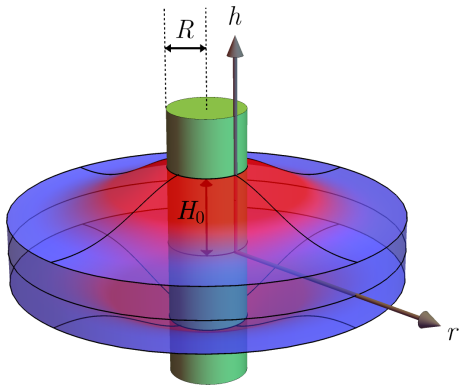

FIG. 1. Schematic of bilayer-protein hydrophobic matching in heterogeneous bilayers. We consider a membrane protein with an approximately cylindrical hydrophobic surface of radius R and height $2H_0$ at the center of an axisymmetric lipid bilayer patch composed of two lipid species with distinct unperturbed hydrophobic thicknesses (lipid species indicated in red and blue). The inner boundary of the lipid bilayer annulus in the membrane patch is constrained by the membrane protein at the center of the membrane patch, while we allow the outer boundary of the membrane patch to be either free or constrained by other proteins. We denote the hydrophobic thickness of the lipid bilayer leaflets by h and the radial coordinate about the protein center by r.

representing the local lipid environment of the membrane protein (see Fig. 1). We take the local lipid environment of the membrane protein to be approximately axisymmetric about the protein center. Furthermore, we assume up-down symmetry in the hydrophobic thickness and composition of the upper and lower lipid bilayer leaflets. Models assuming such an idealized, symmetric lipid bilayer environment have been employed successfully to describe the coupling of membrane protein conformational state and lipid bilayer thickness in homogeneous bilayers [15,19–23] as well as bilayer-thickness-mediated protein interactions in homogeneous bilayers [16,24–36].

In particular, previous work on MscL in homogeneous bilayers [14,17,18,21,22] has suggested that the energetic cost of MscL-induced bilayer thickness deformations dominates the MscL gating energy. MscL was thereby modeled as an axisymmetric, cylindrical membrane protein that induces bilayer thickness deformations in the surrounding membrane [17,18,22]. Other types of membrane proteins may induce distinct modes of bilayer deformation. For instance, Piezo ion channels induce strong midplane deformations in the lipid bilayer [66–68]. Furthermore, membrane proteins do not, in general, show smooth rotational symmetry about the central (transmembrane) protein axis, which can have substantial effects on bilayer-protein interactions [26–28,33,35,43,69]. Here we focus on azimuthally uniform bilayer thickness deformations, and model proteins as cylindrical membrane inclusions (Fig. 1). Further simplification of the modeling approach employed here can be achieved through an effectively one-dimensional version of this model, which we explore in Appendixes A and B.

A. Energy of protein-induced bilayer thickness deformations in heterogeneous lipid bilayers

Protein-induced lipid bilayer thickness deformations tend to decay rapidly away from the lipid-protein boundary, with a decay length ≈1 nm [18,54], tend to be small compared to the unperturbed lipid bilayer thickness, and tend to show small gradients [20,22,28,44] (Fig. 1). As a result, it is useful to describe protein-induced lipid bilayer thickness deformations by expanding the Monge representation of the elastic bilayer deformation energy to leading order in $(h-a)$ and its derivatives [16,24,28,70], where h is the hydrophobic thickness of the lipid bilayer leaflet at the Cartesian coordinates (x, y) and a is the unperturbed hydrophobic thickness of the lipid bilayer leaflet, which depends on the lipid chain length (Fig. 1). The elastic thickness deformation energy of the lipid bilayer can then be written in the form [15–17,22,24–28,44,54]

$$G_h = \int dx\, dy \left\{ \frac{K_b}{2}(\nabla^2 h)^2 + \frac{K_t}{2}\left(\frac{h-a}{a}\right)^2 + \frac{\tau}{2}\left[(\nabla h)^2 + 2\left(\frac{h-a}{a}\right)\right] + \frac{\tau^2}{2K_t}\right\}, \tag{1}$$

where the integral runs over the (in-plane) lipid bilayer surface, K_b is the lipid bilayer bending rigidity, K_t is the bilayer thickness deformation modulus, and τ is the (lateral) membrane tension. For a given lipid composition, the values of the parameters K_b, K_t, and a in Eq. (1) can be measured directly in experiments [12,17,18]. We have added the constant term $\tau^2/2K_t$ in the integrand in Eq. (1) such that $G_h = 0$ for all extremal functions of G_h corresponding to a constant $h(x, y)$ [28].

We consider here protein-induced lipid bilayer thickness deformations in heterogeneous bilayer membranes that effectively consist of two lipid species with distinct unperturbed hydrophobic thicknesses, in a regime in which the two lipid species can form distinct domains with rapid lateral diffusion of lipids in the plane of the membrane [1–7,40,50,51]. At the mean-field level, lipid domain formation in such a binary system is successfully described by the LG free energy [39,40,47,50–52]

$$G_c = \int dx\, dy \left[\frac{\varepsilon}{2}(\nabla c)^2 + \phi(c) - \mu c + \mu_0\right], \tag{2}$$

where the integral runs over the (in-plane) lipid bilayer surface, $c(x, y)$ is a continuous function describing the (mean) lipid composition at the Cartesian coordinates (x, y) such that $c = 0$ and $c = 1$ correspond to the two lipid species under consideration, the parameter ε specifies the energy penalty associated with lipid domain boundaries, the function $\phi(c)$ is the (even) mean-field potential associated with lipid phase separation, and μ is the (local) lipid chemical potential. In analogy to Eq. (1), we include in the integrand in Eq. (2) the constant term $\mu_0 = (|\mu| + \mu)/2$, where $|\mu|$ denotes the absolute value of μ, such that $G_c \geqslant 0$ for all extremal functions of G_c corresponding to a constant lipid composition $c(x, y) = 0$ or $c(x, y) = 1$. The chemical potential μ in Eq. (2) allows for a breaking of the symmetry between $c = 0$ and $c = 1$ in Eq. (2), and locally biases the lipid composition of the membrane patch under consideration towards a particular lipid species. For $\mu = 0$ in Eq. (2) we recover the scenario we considered previously [38], which corresponds to situations in which lipids of either species can freely diffuse into and out of the membrane patch without any external constraints on the lipid composition of the membrane patch.

Following previous work [47,50,71], we consider for the mean-field potential $\phi(c)$ in Eq. (2) a fourth-order polynomial in c centered at $c = 1/2$:

$$\phi(c) = b_0 - \frac{b_1}{2}\left(c - \frac{1}{2}\right)^2 + \frac{b_2}{4}\left(c - \frac{1}{2}\right)^4. \tag{3}$$

The mean-field potential in Eq. (3) can be derived [47,50,71] by expanding additive contributions to the bilayer free energy due to lipid mixing, which oppose lipid domain formation, and lipid-lipid interactions, which favor lipid domain formation. From the LG theory of lipid domain formation [50] we have $b_1 = 4n_0 k_B T/3$ and $b_2 = 16 n_0 k_B T/3$, where n_0 is the mean lipid number per unit area, so that the mean-field potential in Eq. (2) has minima at $c = 0$ and $c = 1$. Furthermore, we set $b_0 = n_0 k_B T/12$ so that the mean-field potential in Eq. (2) is zero at these two minima. The two key physical parameters entering Eq. (2) are thus ε and n_0. We follow here the phenomenological approach in Refs. [40,50] and use, unless specified otherwise, the order-of-magnitude estimates $\varepsilon \sim 1\ k_B T$ and $n_0 \sim 1\ \mathrm{nm}^{-2}$, which were found previously to successfully describe lipid domain formation in bilayers composed of distinct lipid species [39,51,52]. These phenomenological estimates of ε and n_0 yield a lipid-lipid line tension $\sim 0.5\ k_B T/\mathrm{nm}$ that is of the same order of magnitude as the lipid-lipid line tension estimated in experiments on lipid domain formation in giant unilamellar vesicles [72].

We obtain the total bilayer (free) energy of the membrane patch, G, by adding Eqs. (1) and (2):

$$G = G_h + G_c. \tag{4}$$

The fields describing the lipid leaflet thickness, $h(x, y)$, and the lipid bilayer composition, $c(x, y)$, in Eq. (4) are, in principle, coupled [39,40] via the elastic parameters K_b, K_t, and a in Eq. (1), which all depend on the lipid composition [12,17,18].

A variety of experiments on membranes with heterogeneous hydrophobic thickness [1–3,55–57] indicate that lipid bilayer and protein composition couple through hydrophobic lipid-protein interactions driven by differences in the energetically preferred hydrophobic thickness of lipids and membrane proteins, suggesting that a in Eq. (1) provides the dominant coupling of h and c. Based on the experimental data on the dependence of bilayer elastic properties on lipid composition compiled in Ref. [12], we explore in Appendix C the relative importance of the dependence of K_b, K_t, and a in Eq. (1) on lipid composition [17,18]. For all the scenarios considered here we find that the dependence of a on c dominates over the dependence of K_b and K_t on c. We therefore focus on the coupling of h and c through $a(c)$ [39,40]. Notably, experiments show that a depends crucially on the lipid chain length [12]. A major lipid component of cell membranes is provided by phospholipids, for which a roughly varies from $a \approx 1.7$ nm to $a \approx 2.2$ nm for the approximate range in lipid chain length relevant for cell membranes [1–3,12]. Following Refs. [12,22,38,44] we approximate $a(c)$ by a linear function.

We identify the two lipid species in the bilayer with $a(c = 0) = 1.7$ nm (lipid species A) and $a(c = 1) = 2.2$ nm (lipid species B), in which case we have

$$a(c) \approx \alpha_1 c + \alpha_0, \tag{5}$$

where $\alpha_1 = 0.5$ nm and $\alpha_0 = 1.7$ nm [12,22,38,44]. Unless stated otherwise, we use the fixed values $K_b = 20\ k_BT$ and $K_t = 60\ k_BT/\text{nm}^2$ typical for phospholipid bilayer membranes [12,18]. Appendix C considers expressions analogous to Eq. (5) for K_b and K_t.

B. Energy minimization and boundary conditions

We assume that the dominant configurations of the lipid leaflet thickness field $h(x, y)$ and the lipid bilayer composition field $c(x, y)$ minimize the functional G in Eq. (4) with Eqs. (1)–(3) subject to suitable boundary conditions. To determine the minimal $h(x, y)$ and $c(x, y)$ of G, it is convenient to write the total energy in Eq. (4) in polar coordinates such that the fields h and c only depend on the radial coordinate $r = \sqrt{x^2 + y^2}$. The integrands in Eq. (1) and (2) are easily transformed to polar coordinates by noting that, for rotationally symmetric systems such as considered here, $\nabla h = \frac{dh}{dr}\hat{\mathbf{r}}$ and $\nabla c = \frac{dc}{dr}\hat{\mathbf{r}}$, where $\hat{\mathbf{r}}$ is the radial unit vector, and $\nabla^2 h = \frac{1}{r}\frac{d}{dr}(r\frac{dh}{dr})$. We minimize G in the domain $R \leqslant r \leqslant R + L$ (Fig. 1), where L is the width of the lipid bilayer annulus in the membrane patch. To this end, it is useful to write G in the form

$$G = 2\pi \int_R^{R+L} g(r) r\, dr, \tag{6}$$

where $g(r)$ is the lipid bilayer energy density. We numerically minimize G in Eq. (6) using the L-BFGS-B solver [73,74]. Appendix D provides a detailed discussion of the numerical approach employed here, and compares the results obtained using the L-BFGS-B solver to the corresponding results obtained by numerical solution of the Euler-Lagrange equations associated with Eq. (4), which we found to provide a less convenient mathematical approach for the minimization of G. To calculate protein interaction potentials $G_{\text{int}}(L)$ in heterogeneous lipid bilayers, we subtract from the total bilayer energy G in Eq. (4) the G obtained in the large-L, noninteracting regime (see Appendix E).

The mathematical form of the bilayer boundary conditions associated with G in Eq. (4) follows from the calculus of variations [75,76]. In particular, we can have natural (free) or fixed-value boundary conditions on $h(r)$, $\nabla h(r)$, and $c(r)$ at $r = R$ and $r = R + L$. At a boundary $r = r_b$, with $r_b = R$ or $r_b = R + L$, the natural boundary conditions on $h(r)$, $\nabla h(r)$, and $c(r)$ are given by

$$\left\{\frac{d}{dr}\left[\tau h - K_b \frac{1}{r}\frac{d}{dr}\left(r\frac{dh}{dr}\right)\right]\right\}_{r=r_b} = 0, \tag{7a}$$

$$\left[\frac{1}{r}\frac{d}{dr}\left(r\frac{dh}{dr}\right)\right]_{r=r_b} = 0, \tag{7b}$$

$$\left.\frac{dc}{dr}\right|_{r=r_b} = 0, \tag{7c}$$

respectively. With natural boundary conditions, the values of $h(r)$, $\nabla h(r)$, or $c(r)$ at $r = r_b$ can be adjusted as part of the energy minimization. Conversely, the fixed-value boundary conditions on $h(r)$, $\nabla h(r)$, and $c(r)$ at a boundary $r = r_b$ are given by

$$h(r_b) = H_b, \tag{8a}$$

$$\left.\frac{dh}{dr}\right|_{r=r_b} = s_b, \tag{8b}$$

$$c(r_b) = c_b, \tag{8c}$$

respectively, where H_b, s_b, and c_b take given, fixed values.

In principle, one can have any combination of the natural and fixed-value boundary conditions on $h(r)$, $\nabla h(r)$, and $c(r)$ in Eqs. (7a)–(7c) and Eqs. (8a)–(8c) at $r_b = R$ and $r_b = R + L$. The specific form of the boundary conditions used for a given scenario encodes some of the key physical properties of the particular system at hand. We first note that it is energetically very unfavorable to expose the hydrophobic surfaces of lipids or membrane proteins to water while, in general, membrane proteins are considerably more rigid than lipid bilayers [15,17–20,22,44,54]. As a result, one expects that a given conformational state of a membrane protein imposes a given bilayer leaflet thickness H_b at the bilayer-protein boundary. Throughout this article, we therefore use Eq. (8a) at bilayer-protein interfaces. We explore the possible response of membrane proteins to (substantial) bilayer-protein hydrophobic mismatch by, on the one hand, studying the dependence of the bilayer energy on the protein hydrophobic thickness. Such a variable protein hydrophobic thickness could, for instance, originate from a tilting of transmembrane helices. On the other hand, we allow for different conformational states of membrane proteins with distinct hydrophobic thickness, and study the effect of bilayer composition and organization on the thermodynamic competition between these states. In particular, we employ here MscL as a model system to explore lipid-protein organization and regulation through membrane thickness deformations. The closed and open conformational states of MscL yield the approximate hydrophobic thicknesses $H^c = 1.9$ nm and $H^o = 1.3$ nm, respectively, with the approximate protein radii $R^c = 2.5$ nm and $R^o = 3.5$ nm in the closed and open conformational states of MscL [13,14,22,44,54], which we use as reference values for H_b in Eq. (8a) and R.

The choice of the boundary condition on ∇h at bilayer-protein interfaces has been a matter of debate, with some studies suggesting the natural boundary condition in Eq. (7b) and other studies suggesting the fixed-value boundary condition in Eq. (8b) with $s_0 = 0$ [15,20,22,44,54,69]. We use here Eq. (8b) with $s_0 = 0$ at bilayer-protein interfaces. We consider both the natural and fixed-value boundary conditions on c in Eqs. (7c) and (8c) at bilayer-protein interfaces, respectively, with $c_b = 0$ or $c_b = 1$. The former boundary condition corresponds to nonspecific lipid-protein interactions, while the latter boundary condition corresponds to a lipid-protein chemical affinity driven by preferential interactions between particular lipid and protein species. Finally, for scenarios where the (outer) boundary of the membrane patch under consideration is not constrained by membrane proteins, we

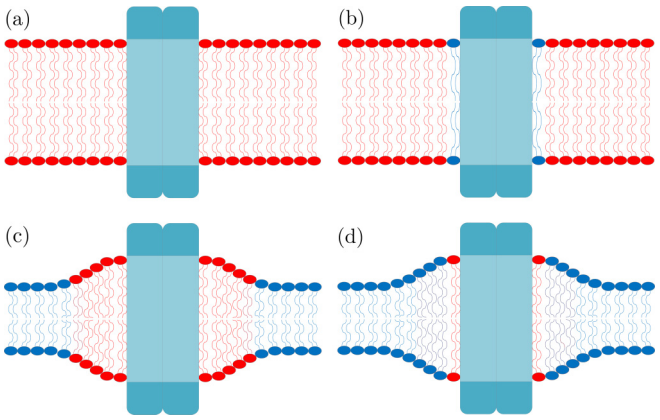

FIG. 2. Illustration of the local lipid environment of a single-membrane protein with (a) zero chemical potential and no chemical affinity between the membrane protein and a particular lipid species, (b) zero chemical potential with a chemical preference of the membrane protein for a particular lipid species (indicated in blue), (c) a nonzero chemical potential with no chemical affinity between the membrane protein and a particular lipid species, and (d) a nonzero chemical potential with a chemical preference of the membrane protein for a particular lipid species (indicated in red). For ease of visualization, we took here one lipid species (indicated in red) to yield an unperturbed hydrophobic bilayer thickness that is identical to the hydrophobic thickness of the membrane protein at the center of the membrane patch.

use the natural boundary conditions in Eqs. (7a)–(7c) for h, ∇h, and c.

III. LIPID-PROTEIN DOMAINS IN DILUTE MEMBRANES

This section focuses on lipid-protein organization and regulation through membrane thickness deformations for a single-membrane protein in a heterogeneous lipid bilayer composed of two lipid species with distinct unperturbed hydrophobic thicknesses. It is useful to distinguish here between four basic scenarios, which are illustrated in Fig. 2. First, we consider the case of zero chemical potential in Eq. (2) with no chemical affinity between the membrane protein at the center of the membrane patch and a particular lipid species [see Fig. 2(a)], for which lipid-protein organization is driven solely by the energetics of lipid bilayer thickness deformations [38]. Second, we consider the case of zero chemical potential in Eq. (2) with a chemical preference of the membrane protein at the center of the membrane patch for a particular lipid species [see Fig. 2(b)]. If the preferred lipid species yields an unperturbed bilayer thickness that is distinct from the hydrophobic thickness of the membrane protein, such a chemical affinity frustrates hydrophobic lipid-protein interactions. Third, we consider the case of a nonzero chemical potential in Eq. (2) with no chemical affinity between the membrane protein at the center of the membrane patch and a particular lipid species [see Fig. 2(c)]. Similarly to Fig. 2(a), the energetics of protein-induced lipid bilayer thickness deformations can then yield, driven by local matching of bilayer and protein hydrophobic thickness, local segregation of a particular lipid species around the membrane protein. Finally, we allow for an interplay of bilayer thickness deformations with a nonzero chemical potential in Eq. (2) and a chemical affinity between particular lipid and protein species [see Fig. 2(d)], which can perturb the lipid-protein organization obtained from a local matching of bilayer and protein hydrophobic thickness.

Since we focus here on a single-membrane protein in a heterogeneous lipid bilayer membrane we use, throughout this section, the natural boundary conditions in Eqs. (7a)–(7c) at the (outer) membrane patch boundary $r_b = R + L$. Furthermore, we choose membrane patch sizes large enough so that $g(R + L) \approx 0$ in Eq. (6). We first consider how lipid-protein organization and the energy of protein-induced lipid bilayer thickness deformations depend on the membrane protein hydrophobic thickness with and without a chemical affinity between the membrane protein and a particular lipid species, at zero chemical potential in Eq. (2) and at zero membrane tension in Eq. (1) (see Sec. III A). We then allow for a nonzero chemical potential in Eq. (2), which effectively biases the composition of the lipid bilayer patch towards a particular lipid species, and explore the effects of such a bias on lipid-protein organization and the energy of protein-induced lipid bilayer thickness deformations, again at zero membrane tension in Eq. (1) (see Sec. III B). Finally, we consider the effects of a nonzero membrane tension in Eq. (1) on protein-induced lipid bilayer thickness deformations in heterogeneous bilayers (see Sec. III C). In particular, using MscL as a model system, we study how heterogeneity in the preferred bilayer hydrophobic thickness affects the tension-dependent gating of ion channels. We find that, even at fixed (low) membrane tension, changes in lipid heterogeneity can induce MscL gating.

A. Lipid-protein chemical affinity

Figure 3 contrasts lipid-protein organization and the energy of protein-induced lipid bilayer thickness deformations for scenarios without and with a chemical affinity between particular lipid and protein species [Figs. 2(a) and 2(b)]. A detailed discussion of the former scenario is provided in Ref. [38]. Throughout this section we assume zero membrane tension in Eq. (1) and zero chemical potential in Eq. (2). For general values of the hydrophobic thickness of the membrane protein at the center of the membrane patch, $H_b = H_0$, we find that a chemical affinity between the membrane protein and a particular lipid species only has a minor effect on the overall lipid composition of the bilayer patch surrounding the membrane protein, with the average lipid composition of the bilayer patch being driven primarily by the interplay of lipid and protein hydrophobic thickness [38]. However, we also find that, if the hydrophobic thickness of the membrane protein (or of the lipids) is tuned to lie within a certain (narrow) range, modification of the lipid-protein chemical affinity can have a dramatic effect on the lipid composition of the membrane patch. For instance, for the parameter values used for Fig. 3 we find that two proteins with similar hydrophobic thicknesses within the range 1.91 nm $\lessapprox H_0 \lessapprox$ 1.98 nm but different chemical affinities—one for lipid species A ($c_b = c_0 = 0$) and the other for lipid species B ($c_b = c_0 = 1$)—can yield markedly different lipid compositions of the membrane patch, with the membrane patch composition being dominated by either lipid species A or B [see Fig. 3(a)].

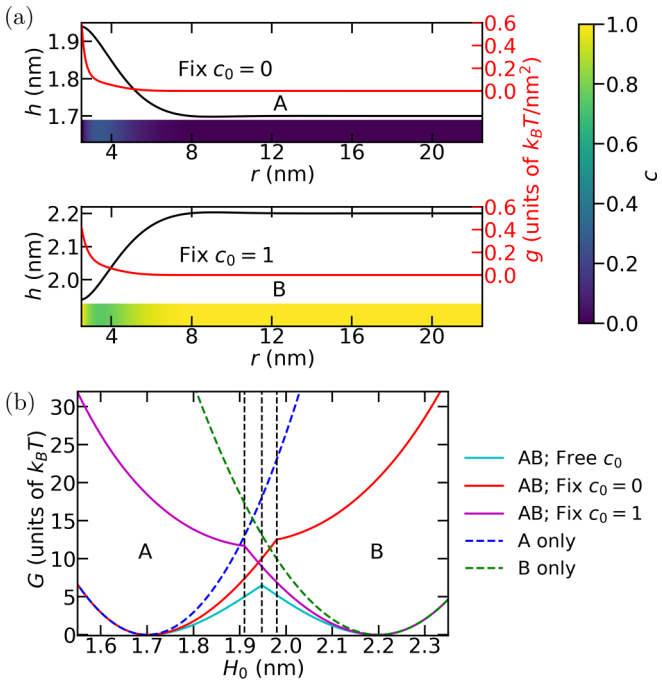

FIG. 3. Lipid-protein organization for a single-membrane protein with and without a lipid-protein chemical affinity. (a) Bilayer leaflet thickness profile h (left axes), lipid composition c (color bars), and energy density g in Eq. (6) (right axes) for the fixed-value boundary conditions $c(R) = c_0$ with $c_0 = 0$ (upper panel) and $c_0 = 1$ (lower panel) as a function of the radial coordinate r at $H_0 = 1.94$ nm. (b) Total bilayer energy G in Eq. (4) as a function of H_0 for a heterogeneous bilayer containing lipid species A and B and homogeneous bilayers composed solely of lipid species A or B for natural boundary conditions on c at $r = R$ or the indicated lipid-protein affinities. The dashed vertical lines show $H_0 = H_0^*$ for fixed $c_0 = 0$, free c_0, and fixed $c_0 = 1$ (right to left), for which the dominant lipid composition in the membrane patch changes sharply from lipid species A to lipid species B. At $r = R + L$ we use, for all panels, the natural boundary conditions in Eqs. (7a)–(7c). We set $L = 20$ nm, $R = R^c$, $\mu = 0$, and $\tau = 0$.

For membrane proteins without a chemical affinity for a particular lipid species, changes in the protein hydrophobic thickness H_0 across a critical value H_0^* yield a sharp change in the lipid composition of the bilayer patch [38] [see Fig. 3(b)]. A similar transition in lipid composition is obtained for membrane proteins that have a chemical affinity for a particular lipid species, but at different values of H_0^* [Fig. 3(b)]. For instance, for the parameter values used for Fig. 3, we have $H_0^* = 1.95$ nm for natural boundary conditions on c at the bilayer-protein interface, but $H_0^* = 1.98$ nm and $H_0^* = 1.91$ nm for the fixed-value boundary conditions $c_0 = 0$ and $c_0 = 1$, respectively. Furthermore, a chemical affinity between particular lipid and protein species dramatically affects the energy landscape of lipid-protein interactions [Fig. 3(b)]. Notably, G shows minima at both $H_0 = a(0)$ and $H_0 = a(1)$ for natural boundary conditions on c at the bilayer-protein interface. In contrast, fixed-value boundary conditions on c at the bilayer-protein interface yield a unique minimum of G at $H_0 = a(c_0)$.

The foregoing results can be understood intuitively by noting that, in the case of a (strong) chemical affinity between particular lipid and protein species, the lipids at the bilayer-protein boundary deviate from their preferred hydrophobic thickness if $H_0 \neq a(c_0)$, yielding a frustrated bilayer-protein configuration. However, since gradients in c are energetically unfavorable, the membrane patch maintains an approximately uniform lipid composition with $c \approx c_0$, as long as $H_0 \approx a(c_0)$. But, if H_0 deviates strongly enough from $a(c_0)$, the energetics of bilayer thickness deformations can make it favorable for the lipid bilayer composition to rapidly transition around the membrane protein to a composition $c \neq c_0$, yielding a dominant lipid composition of the membrane patch that is distinct from c_0, with substantial bilayer thickness deformations and substantial $|\nabla c|$ in the immediate vicinity of the membrane protein.

B. Lipid chemical potential

A nonzero chemical potential μ introduces an external bias to the lipid composition of the membrane patch. Such an external bias may arise through interactions of the membrane patch with the surrounding membrane in which, for instance, one lipid species may be dominant overall. A nonzero chemical potential μ competes with bilayer thickness deformations and/or a chemical affinity between particular lipid and protein species to drive lipid-protein organization [Figs. 2(c) and 2(d)]. For example, for a membrane protein with a hydrophobic thickness $H_0 = 1.7$ nm matching the unperturbed bilayer leaflet thickness associated with lipid species A and no lipid-protein chemical affinity, the membrane patch only contains lipids of species A for $\mu = 0$. However, as μ is increased from zero, the lipid bilayer composition is increasingly biased towards lipid species B, eventually resulting in the localization of lipid species A in the immediate vicinity of the membrane protein, with the overall lipid composition of the membrane patch being dominated by lipid species B [see Fig. 4(a)]. For moderate values of $|\mu|$, the total bilayer energy of the membrane patch, G in Eq. (4), shows two minima as a function of H_0 corresponding to lipid species A and B, respectively, with the minimum associated with lipid species A providing the global energy minimum for $\mu < 0$, and vice versa [see Fig. 4(b)]. As $|\mu|$ is increased, the energy landscape of the membrane patch approaches that associated with a membrane patch containing only lipids of species A or B, yielding a unique energy minimum at $H_0 \approx a(0)$ or $H_0 \approx a(1)$ [Fig. 4(b)].

The competition between a nonzero chemical potential, bilayer thickness deformations, and a chemical affinity between particular lipid and protein species can produce a variety of scenarios for lipid-protein organization [see Figs. 4(c) and 4(d)]. For instance, the external chemical potential may compete with lipid-protein affinity, thereby frustrating lipid-protein organization. In this case, the lipid composition of the membrane patch in the immediate vicinity of the membrane protein is determined by the chemical preference of the membrane protein for a particular lipid species, while the lipid composition of the membrane patch away from the membrane protein is dominated by the competition between the external chemical potential and bilayer thickness

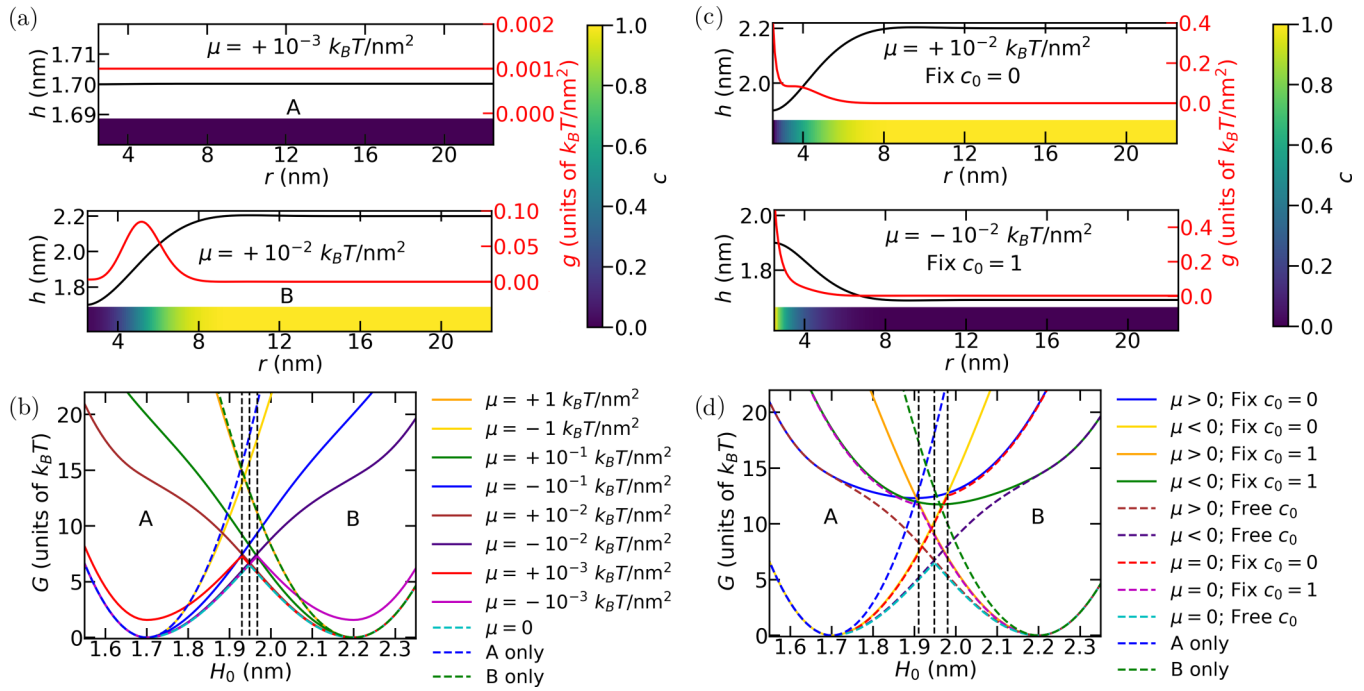

FIG. 4. Dependence of lipid-protein organization on the membrane patch chemical potential μ, in the case of a single-membrane protein. Bilayer leaflet thickness profile h (left axes), lipid composition c (color bars), and energy density g in Eq. (6) (right axes) for (a) natural boundary conditions on c at the bilayer-protein interface and $H_0 = 1.7$ nm with $\mu = 10^{-3}\ k_BT/\text{nm}^2$ (upper panel) and $\mu = 10^{-2}\ k_BT/\text{nm}^2$ (lower panel), and (c) the fixed-value boundary condition $c(R) = c_0$ at the bilayer-protein interface and $H_0 = 1.9$ nm with $c_0 = 0$, $\mu = 10^{-2}\ k_BT/\text{nm}^2$ (upper panel) and $c_0 = 1$, $\mu = -10^{-2}\ k_BT/\text{nm}^2$ (lower panel). Total bilayer energy G in Eq. (4) as a function of H_0 for a heterogeneous bilayer containing lipid species A and B and homogeneous bilayers composed solely of lipid species A or B for the indicated values of μ with (b) natural boundary conditions on c at the bilayer-protein interface and (d) the indicated fixed-value boundary conditions on c at the bilayer protein interface with $\mu = \pm 10^{-2}\ k_BT/\text{nm}^2$ ($\mu \gtrless 0$) (curves corresponding to free c_0 included for reference). In panel (b), the dashed vertical lines show $H_0 = H_0^*$ for free c_0 at $\mu = 10^{-3}\ k_BT/\text{nm}^2$, $\mu = 0$, and $\mu = -10^{-3}\ k_BT/\text{nm}^2$ (right to left), for which the dominant lipid composition in the membrane patch changes sharply from lipid species A to lipid species B. Similarly, the gray dashed vertical lines in panel (d) show $H_0 = H_0^*$ for $c_0 = 0$, free c_0, and $c_0 = 1$ at $\mu = 0$ (right to left). At $r = R + L$ we use, for all panels, the natural boundary conditions in Eqs. (7a)–(7c). We set $L = 20$ nm, $R = R^c$, and $\tau = 0$ for all panels.

deformations [Fig. 4(c)]. Examining G in Eq. (4) as a function of H_0 we find a unique energy minimum for large enough $|\mu|$ that neither corresponds to the unperturbed hydrophobic thickness associated with lipid species A nor to the unperturbed hydrophobic thickness associated with lipid species B [Fig. 4(d)]. However, this minimum in $G(H_0)$ can be rather shallow, suggesting strong fluctuations in the lipid-protein organization in this regime, with no sharp transition in the lipid composition of the membrane patch as H_0 is varied.

C. Gating of ion channels in heterogeneous bilayers

The results in Figs. 3 and 4 show that heterogeneity in the unperturbed lipid bilayer thickness can have a pronounced effect on the energy of protein-induced lipid bilayer thickness deformations. For conformational transitions in membrane proteins that involve a change in protein hydrophobic thickness [15,17–23], lipid heterogeneity is therefore expected to bias the protein conformation towards particular states. We illustrate here the regulation of protein function through heterogeneity in the unperturbed lipid bilayer thickness using the tension-dependent gating of MscL as a model system. The experimental phenomenology of MscL is captured by a two-state model, in which MscL is assumed to be either in closed or open conformational states with gating probability

$$P_o = \frac{1}{1 + e^{(\Delta G - \tau \Delta A)/k_BT}}, \tag{9}$$

where $\Delta G = G^o - G^c$ is the energy difference between the open and closed states of MscL and $\Delta A = \pi[(R^o)^2 - (R^c)^2]$ is the change in (in-plane) membrane area. The gating energy ΔG involves contributions due to internal protein conformational changes as well as bilayer-protein interactions.

Remarkably, the basic experimental phenomenology of MscL gating in homogeneous bilayer membranes can already be captured based solely on contributions to ΔG arising from bilayer thickness deformations [21,22,44,54]. We consider here MscL gating in heterogeneous lipid bilayers [38], and calculate ΔG from Eq. (4) for the open and closed states of MscL, using the boundary conditions described in Sec. II B. To quantify MscL gating, we define the MscL gating tension $\bar{\tau}$ as the smallest membrane tension τ with $P_o \geqslant 1/2$. Experiments on MscL gating in *Escherichia coli* giant spheroplasts have yielded an estimate $\bar{\tau} \approx 2.5\ k_BT/\text{nm}^2$ [54,77], but $\bar{\tau}$ is known to depend on the lipid bilayer composition [9,21,22,44]. While there is, to our knowledge, currently no experimental evidence demonstrating a strong chemical affinity between (closed- or open-state) MscL and a particular

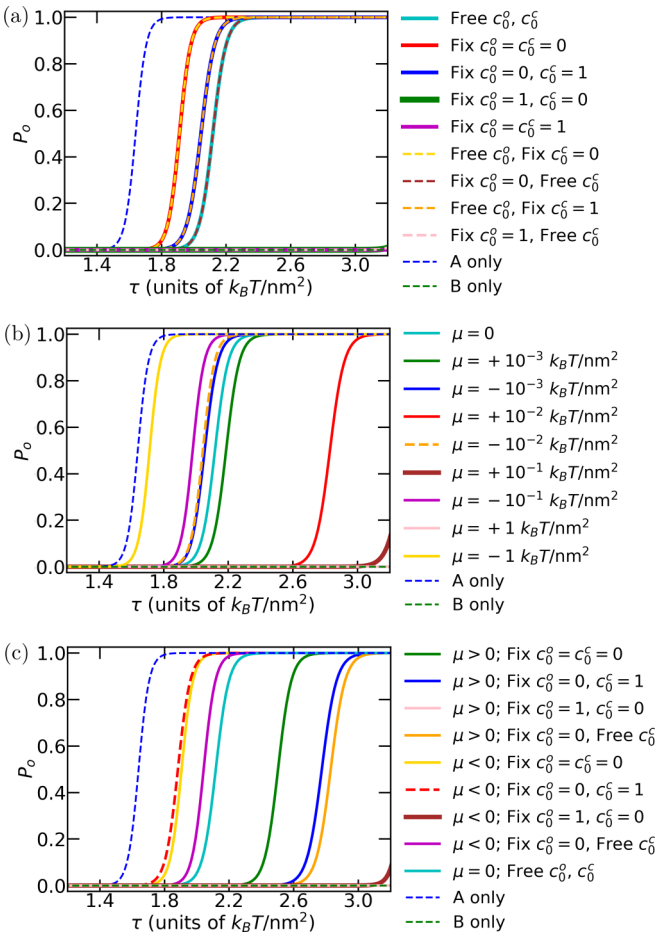

FIG. 5. Gating of single MscL in heterogeneous lipid bilayers. MscL gating probability P_o in Eq. (9) as a function of membrane tension τ for heterogeneous bilayers composed of lipid species A and B for (a) $\mu = 0$ with natural boundary conditions on c at the bilayer-MscL interface or the indicated values of c_0 in the closed ($c_0 = c_0^c$) and open ($c_0 = c_0^o$) conformational states of MscL, (b) $\mu \neq 0$ with natural boundary conditions on c at the bilayer-MscL interface, and (c) $\mu \neq 0$ with various combinations of free and fixed boundary conditions on c for the closed and open conformational states of MscL. In panel (c) we use $\mu = \pm 10^{-2}\ k_BT/\text{nm}^2$ ($\mu \gtrless 0$). For reference, we show in all panels the corresponding results obtained for $\mu = 0$ with natural boundary conditions on c at the bilayer-MscL interface [38], and for homogeneous bilayers composed solely of lipid species A or B.

lipid species, MscL could be modified to synthetically engineer such an affinity and, more generally, a great variety of other membrane proteins have been found to show chemical affinities for particular lipid species [61–65].

We have shown previously [38] that, for zero chemical potential and no lipid-protein chemical affinity, lipid bilayer heterogeneity can produce shifts in $\bar{\tau}$ that are a substantial fraction of the bilayer rupture tension $\tau_r \approx 3\ k_BT/\text{nm}^2$ [54]. Here we find that a lipid-protein chemical affinity [see Fig. 5(a)], a nonzero chemical potential [see Fig. 5(b)], or a combination of both effects [see Fig. 5(c)] can further modify MscL gating, with a complex dependence of $\bar{\tau}$ on the lipid bilayer properties. For instance, Fig. 5(a) suggests that, if MscL shows an affinity for a particular lipid species in its closed state but not in its open state, the gating tension of MscL is generally lowered, and vice versa. This can be understood intuitively by noting that a lipid-protein affinity increases the constraints on the lipid-protein system, and thus generally increases the energy of protein-induced lipid bilayer thickness deformations. An exception to this rule occurs if the fixed-value boundary condition on c at the bilayer-protein interface is chosen so as to coincide with the value of c implied by the corresponding natural boundary condition on c. Interestingly, Fig. 5(a) shows that, for certain types of lipid-protein affinity, MscL gating is effectively suppressed in the physically relevant tension range $0 \leqslant \tau \leqslant \tau_r$, thus stabilizing MscL in its closed conformational state. This behavior can arise if the chemical affinity of open-state MscL for a particular lipid species yields a lipid composition in the vicinity of MscL that, due to MscL-induced lipid bilayer thickness deformations, is highly unfavorable from an energetic perspective.

In addition to a chemical affinity between MscL and particular lipid species, a nonzero chemical potential can also substantially affect MscL gating [Fig. 5(b)]. In particular, for the parameter values used for Fig. 5(b), $\mu > 0$ tends to increase $\bar{\tau}$ while $\mu < 0$ tends to decrease $\bar{\tau}$. This can be understood intuitively by noting that $H^{(c)} > H^{(o)}$ for MscL [13,14,22,44,54], while lipid species A has a smaller unperturbed hydrophobic thickness than lipid species B. As a result, a bias of the lipid bilayer composition towards lipid species B over lipid species A favors the closed state of MscL over the open state of MscL, and vice versa. Note, however, that the predicted shifts in $\bar{\tau}$ are not symmetric about $\mu = 0$, because the thickness deformation energy in Eq. (1) explicitly depends on $a(c)$. Combining a chemical affinity of MscL for a particular lipid species with a nonzero chemical potential we obtain an intricate dependence of $\bar{\tau}$ on the values of c_0 and μ [see Fig. 5(c)]. For instance, with $\mu > 0$ we find substantial differences in $\bar{\tau}$ for scenarios in which MscL has an affinity for lipid species A in both its open and closed states [green curve in Fig. 5(c)], and in which MscL has an affinity for lipid species A in its open state and an affinity for lipid species B in its closed state [indigo curve in Fig. 5(c)]. In contrast, the MscL gating curves corresponding to these two scenarios are almost identical if the sign of μ is flipped so that $\mu < 0$ [blue and red curves in Fig. 5(c)]. Collectively, we find in Fig. 5 that heterogeneity in the lipid composition of bilayer membranes can, through protein-induced bilayer thickness deformations, lipid-protein chemical affinity, and the local lipid chemical potential, strongly affect the competition between distinct conformational states of membrane proteins.

IV. LIPID-PROTEIN DOMAINS IN CROWDED MEMBRANES

An overlap in the bilayer thickness deformations induced by neighboring membrane proteins gives rise to bilayer-thickness-mediated protein interactions, which can yield self-assembly of supramolecular membrane protein assemblies [16,24–36]. Interestingly, it follows from the mechanics of bilayer thickness deformations [15–17,22,24–28,44,54] that protein-induced bilayer thickness deformations are localized over a scale of approximately 4 nm about each membrane

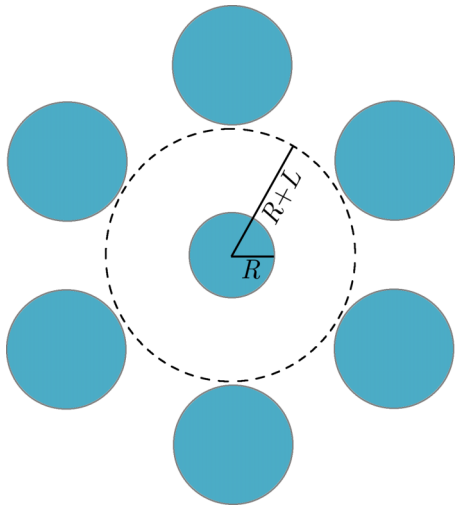

FIG. 6. Schematic of the mean-field model of bilayer-mediated protein interactions in crowded membranes [24,38,70,78–80]. The membrane protein at the center of the membrane patch has radius R and is surrounded by a lipid bilayer annulus of thickness L. The boundary conditions at the outer rim of the bilayer annulus at $r = R + L$ are taken to be axisymmetric about the membrane patch center, and are chosen so as to model a uniform array of membrane proteins (see Sec. II B).

protein, which corresponds to roughly one-half the typical protein-protein separation in cell membranes [4,18]. The interaction of membrane proteins through bilayer thickness deformations may therefore have a broad impact on the local organization and cooperative function of cell membranes. To ascertain the role of bilayer-thickness-mediated protein interactions in cell membrane organization and function, it is important to understand how such protein interactions are modified by the heterogeneous lipid bilayer compositions typically found in cell membranes [1–3,12]. We have previously explored the influence of lipid heterogeneity on membrane protein interactions mediated by bilayer thickness deformations for natural boundary conditions on c at the bilayer-protein interface and zero chemical potential in Eq. (2) [38].

This section focuses on the effects of a nonzero chemical potential in Eq. (2) and a chemical affinity between particular lipid and protein species on bilayer-thickness-mediated protein interactions in heterogeneous lipid bilayers. We employ a mean-field approach [24,38,70,78–80], and consider a membrane protein at the center of a membrane patch surrounded by a uniform array of identical proteins (see Fig. 6). This mean-field approach cannot capture the roles of protein shape and multibody effects in bilayer-thickness-mediated protein interactions [26–28,35] but, based on previous work on membrane protein interactions mediated through thickness deformations in homogeneous bilayers [24], is expected to correctly capture the sign, approximate range, and order of magnitude of bilayer-mediated protein interactions in heterogeneous bilayers. We first consider bilayer-thickness-mediated protein interactions for an array of membrane proteins with a hydrophobic thickness that is identical to (see Sec. IV A) or distinct from (see Sec. IV B) the hydrophobic thickness of the protein at the center of the membrane patch. On this basis, we then investigate protein cooperativity in heterogeneous bilayer membranes (see Sec. IV C). We find that heterogeneity in the lipid chain length can expand the repertoire and range of membrane protein interactions mediated by bilayer thickness deformations, can yield colocalization of lipids and membrane proteins according to their preferred hydrophobic thickness, and can have a pronounced effect on bilayer-mediated protein cooperativity.

A. Proteins with identical hydrophobic thickness

In this section we explore scenarios in which the protein at the center of the membrane patch has a hydrophobic thickness H_0 that is identical to the hydrophobic thickness of the surrounding membrane proteins, $H_L = H_0$ (see Fig. 7). We set here $H_0 = H_L = 2.0$ nm, which lies in between the unperturbed bilayer leaflet thicknesses $a = 1.7$ nm and $a = 2.2$ nm associated with lipids of species A and B, respectively. We first consider situations in which the protein at the center of the membrane patch and its neighboring membrane proteins have chemical affinities for the same [see Fig. 7(a)] or distinct [see Fig. 7(b)] lipid species with zero chemical potential in Eq. (2). Subsequently, we consider bilayer-thickness-mediated protein interactions for situations in which the protein at the center of the membrane patch and its neighboring membrane proteins have natural boundary conditions on c at the bilayer-protein interfaces but $\mu \neq 0$ with, again, $H_L = H_0$ [see Fig. 7(c)]. Comparison of the results in Figs. 7(a), 7(b), and 7(c) with the corresponding results obtained for natural boundary conditions on c at the bilayer-protein interfaces with $\mu = 0$ [38] shows that a chemical preference of the membrane proteins for a particular lipid species or a nonzero chemical potential can produce substantial shifts in bilayer-thickness-mediated protein interactions.

For $c_0 = c_L = 0$, $\mu = 0$, and large L, we find that lipid domains with $c \approx 0$ form near the protein boundaries at $r = R$ and $r = R + L$ [left panel in Fig. 7(a)]. As L is decreased, these domains merge, as also found for membrane proteins with natural boundary conditions on c [38], but the resulting bilayer-thickness-mediated protein interactions $G_{\rm int}(L)$ are not as favorable as in the case of natural boundary conditions on c [right panel in Fig. 7(a)]. This can be understood intuitively by noting that $H_0 = H_L = 2.0$ nm and $c_0 = c_L = 0$ produce substantial bilayer thickness deformations in the vicinity of the proteins, which incurs an energy penalty and produces less favorable interactions at small L. As expected, we find similar, but less pronounced, effects of lipid-protein chemical affinity on lipid organization and bilayer-thickness-mediated protein interactions with $H_0 = H_L = 2.0$ nm and $c_0 = c_L = 1$, for which the bilayer thickness is deformed less strongly in the vicinity of the proteins than for $c_0 = c_L = 0$ [middle and right panels in Fig. 7(a)]. For situations with $c_0 \neq c_L$ and $\mu = 0$, lipid-protein chemical affinity can further reduce the strength of energetically favorable interactions, and even render bilayer-thickness-mediated protein interactions unfavorable for all protein separations considered in Fig. 7(b). This can be understood intuitively by noting that, in this case, distinct lipid-protein affinities at $r = R$ and $r = R + L$ induce distinct lipid environments at $r = R$ and $r = R + L$,

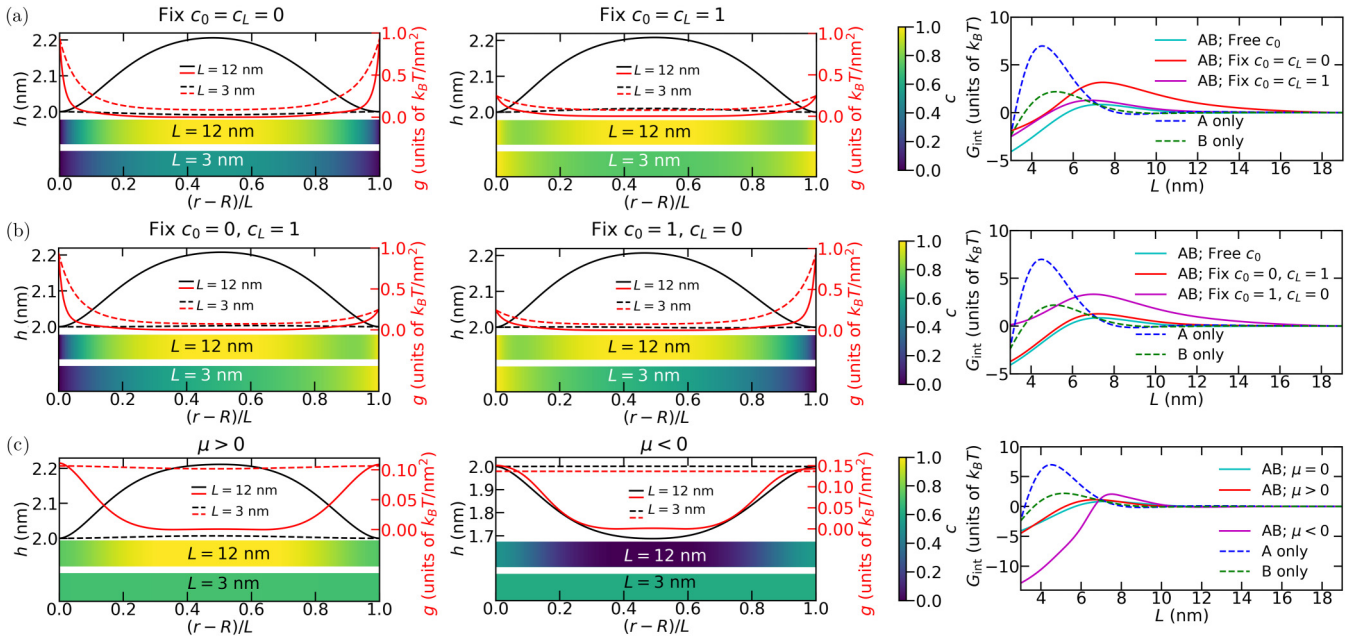

FIG. 7. Bilayer-thickness-mediated protein interactions in heterogeneous bilayers for membrane proteins with identical hydrophobic thickness, $H_0 = H_L$, using $H_0 = H_L = 2.0$ nm. Bilayer leaflet thickness profile h (left axes), lipid composition c (color bars), and energy density g in Eq. (6) (right axes) for $L = 3$ nm and $L = 12$ nm vs $(r - R)/L$ with $R = R^c$ (left and middle panels) and corresponding bilayer-thickness-mediated protein interaction potentials $G_{\rm int}(L)$ (right panels) for (a) fixed-value boundary conditions on c with $c_0 = c_L$ and $\mu = 0$, (b) fixed-value boundary conditions on c with $c_0 \neq c_L$ and $\mu = 0$, and (c) natural boundary conditions on c and $\mu = \pm 10^{-2}\ k_BT/\text{nm}^2$ ($\mu \gtrless 0$). In the right panels we show, for reference, also the $G_{\rm int}(L)$ obtained for natural boundary conditions on c and $\mu = 0$ in heterogeneous bilayers composed of lipid species A and B (AB), as well as the $G_{\rm int}(L)$ obtained for homogeneous bilayers composed solely of lipid species A or B [38]. To calculate $G_{\rm int}(L)$, we subtracted from the total bilayer energy G in Eq. (4) the value of G obtained in the large-L, noninteracting regime (see Appendix E). We set $\tau = 0$ for all panels.

which prevents a merging of lipid domains at small L [left and middle panels in Fig. 7(b)]. Furthermore, we find that, compared to situations with natural boundary conditions on c, fixed-value boundary conditions on c at the bilayer-protein interfaces can substantially increase the range of (unfavorable) bilayer-thickness-mediated protein interactions [right panels in Figs. 7(a) and 7(b)].

In Fig. 7(c) we explore bilayer-thickness-mediated protein interactions for situations in which $\mu < 0$ or $\mu > 0$ in Eq. (2), with $H_0 = H_L$ and natural boundary conditions on c. A positive chemical potential tends to bias the lipid composition of the membrane patch towards lipids of species B, while a negative chemical potential tends to bias the lipid composition of the membrane patch towards lipids of species A. We find that, depending on the interplay of protein hydrophobic thickness, the sign and magnitude of the chemical potential, and the unperturbed bilayer thicknesses associated with the particular lipid species under consideration, a nonzero chemical potential can strongly affect bilayer-thickness-mediated protein interactions [Fig. 7(c)]. For instance, with $H_0 = H_L = 2.0$ nm we find that $\mu = 0$ and $\mu > 0$ give similar interaction potentials, but that $\mu < 0$ gives bilayer-thickness-mediated protein interactions that are much more favorable at intermediate L, and have a somewhat greater range, than obtained with $\mu = 0$ or $\mu > 0$ [Fig. 7(c)]. Note that $\mu < 0$ and $\mu > 0$ (or $\mu = 0$) yield a similar lipid-protein organization at small L, but drastically different lipid bilayer compositions at large L that are dominated by lipid species A and B, respectively [Fig. 7(c)].

B. Proteins with distinct hydrophobic thickness

We consider in this section scenarios in which the protein at the center of the membrane patch has a hydrophobic thickness H_0 that is different from the hydrophobic thickness of the surrounding membrane proteins, $H_L \neq H_0$ (see Fig. 8). In particular, we set $H_0 = 2.2$ nm and $H_L = 1.3$ nm. These values of H_0 and H_L should be contrasted with the unperturbed bilayer leaflet thicknesses $a = 1.7$ nm and $a = 2.2$ nm associated with lipid species A and B, respectively. We thus have perfect hydrophobic matching for the protein at $r = R$ and lipid species B, and a preference of the proteins at $r = R + L$ for lipid species A over lipid species B.

Focusing first on situations with $\mu = 0$ we find that, if $c_L = 1$ so that that lipids at $r = R + L$ are substantially expanded in hydrophobic thickness, bilayer-thickness-mediated protein interactions are more unfavorable and longer in range than in the case of natural boundary conditions on c, irrespective of whether $c_0 = 0$ or $c_0 = 1$ [see Fig. 8(a)]. This can be understood intuitively by noting that, to reduce the energy cost of bilayer thickness deformations, the bilayer composition (rapidly) changes here from lipid species B towards lipid species A as r is decreased from $r = R + L$ for both $c_0 = 0$ and $c_0 = 1$ [see the left and middle panels in Fig. 8(a)], which results in lipid-protein configurations that are increasingly unfavorable as L is decreased. Conversely, if $c_L = 0$ the lipids at $r = R + L$ are not as expanded in hydrophobic thickness as for $c_L = 1$, and we find bilayer-thickness-mediated protein

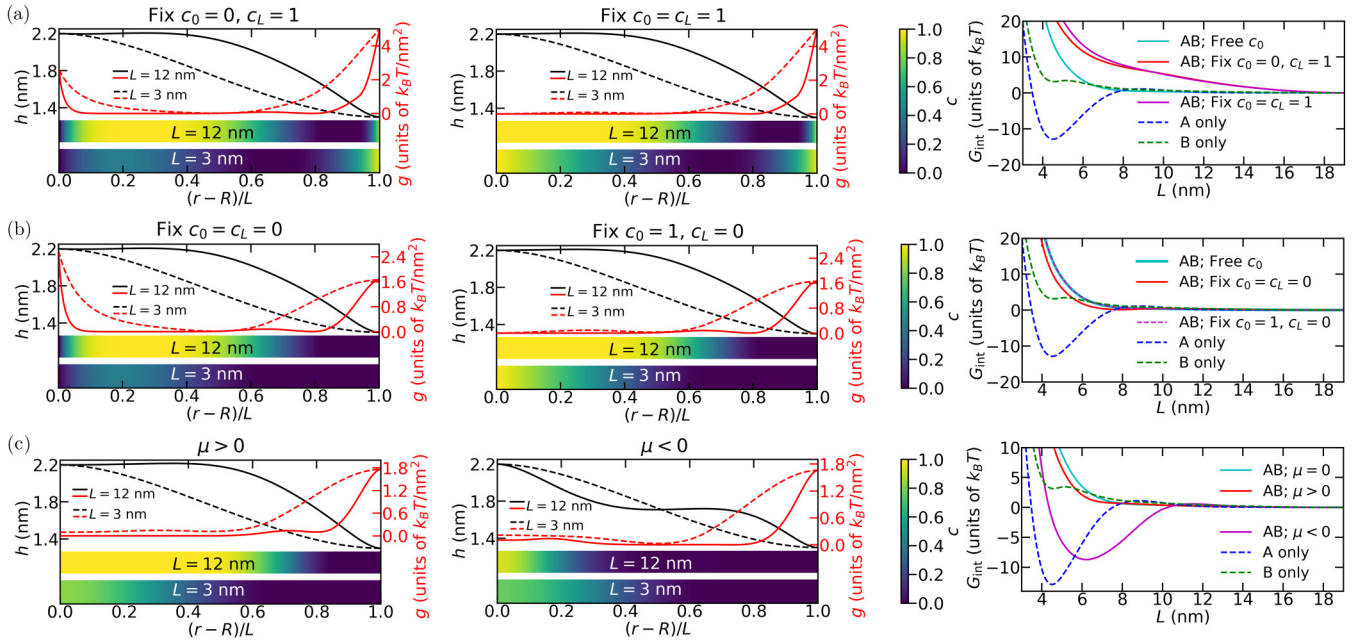

FIG. 8. Bilayer-thickness-mediated protein interactions in heterogeneous bilayers for membrane proteins with distinct hydrophobic thickness, $H_0 \neq H_L$, using $H_0 = 2.2$ nm and $H_L = 1.3$ nm. Bilayer leaflet thickness profile h (left axes), lipid composition c (color bars), and energy density g in Eq. (6) (right axes) for $L = 3$ nm and $L = 12$ nm vs $(r - R)/L$ with $R = R^c$ (left and middle panels) and corresponding bilayer-thickness-mediated protein interaction potentials $G_{\rm int}(L)$ (right panels) for (a) fixed-value boundary conditions on c with $c_0 = 0$ or $c_0 = 1$ and $c_L = 1$ at $\mu = 0$, (b) fixed-value boundary conditions on c with $c_0 = 0$ or $c_0 = 1$ and $c_L = 0$ at $\mu = 0$, and (c) natural boundary conditions on c at $\mu = \pm 10^{-2}\ k_BT/\text{nm}^2$ ($\mu \gtrless 0$). In the right panels we show, for reference, also the $G_{\rm int}(L)$ obtained for natural boundary conditions on c and $\mu = 0$ in heterogeneous bilayers composed of lipid species A and B (AB), as well as the $G_{\rm int}(L)$ obtained for homogeneous bilayers composed solely of lipid species A or B [38]. To calculate $G_{\rm int}(L)$, we subtracted from the total bilayer energy G in Eq. (4) the value of G obtained in the large-L, noninteracting regime (see Appendix E). We set $\tau = 0$ for all panels.

interactions that are similar to those obtained with natural boundary conditions on c, irrespective of whether $c_0 = 0$ or $c_0 = 1$ [see Fig. 8(b)].

In Fig. 8(c) we consider bilayer-thickness-mediated protein interactions for $H_0 = 2.2$ nm and $H_L = 1.3$ nm with natural boundary conditions on c for $\mu < 0$ and $\mu > 0$ in Eq. (2). Similarly as in Fig. 7(c), we find that a nonzero chemical potential can have a pronounced effect on bilayer-mediated protein interactions. In particular, $\mu < 0$ can result, at intermediate L, in a regime with strongly favorable bilayer-mediated protein interactions [right panel in Fig. 8(c)]. In contrast, $\mu = 0$ and $\mu > 0$ both yield unfavorable bilayer-mediated protein interactions for all L in Fig. 8(c). This can be understood intuitively by noting that homogeneous bilayers composed solely of lipid species A yield an energetically favorable interaction regime in Fig. 8(c). Since a negative lipid chemical potential biases the lipid bilayer composition towards lipids of species A, $\mu < 0$ can therefore also yield an energetically favorable interaction regime. Interestingly, for $\mu < 0$ the energetically favorable regime of bilayer-thickness-mediated protein interactions in Fig. 8(c) has a longer range than for homogeneous bilayers composed solely of lipid species A.

C. Protein cooperativity in heterogeneous bilayers

The results in Figs. 7 and 8 show that lipid heterogeneity can have a pronounced effect on bilayer-thickness-mediated protein interactions. This, in turn, suggests that lipid heterogeneity modifies protein cooperativity in the crowded protein environments provided by cell membranes [1–5,18]. In analogy to Sec. III C, we explore here the effect of lipid heterogeneity on protein cooperativity using MscL as a model system. For MscL embedded in lipid bilayers with homogeneous lipid composition, it has been predicted [25] and observed experimentally [32] that MscL gating is affected by protein crowding. As for Figs. 7 and 8, we use the mean-field model in Fig. 6 to explore protein cooperativity in heterogeneous bilayers. Specifically, we take the protein at the center of the membrane patch to correspond to the closed or open state of MscL, and take the neighboring proteins to impose bilayer boundary conditions corresponding to open-state MscL proteins. Employing Eq. (9) with different L we then calculate, as a function of membrane tension, the probability that the MscL protein at the center of the membrane patch is in its open conformational state, P_o, and thus quantify protein cooperativity (see Fig. 9). We denote the protein edge-to-edge separations in the far-field (weakly interacting) and closed-packed (strongly interacting) regimes by $L = L_f$ and $L = L_c$, respectively. We use here $L_f = 12$ nm and $L_c = 3$ nm. We denote the corresponding MscL gating tensions by $\bar{\tau}_f$ and $\bar{\tau}_c$, respectively, which are the smallest values of the membrane tension for which $P_o \geqslant 1/2$.

We first consider how a lipid-MscL chemical affinity affects cooperative gating of MscL in heterogeneous bilayers, at zero chemical potential and assuming that MscL shows the

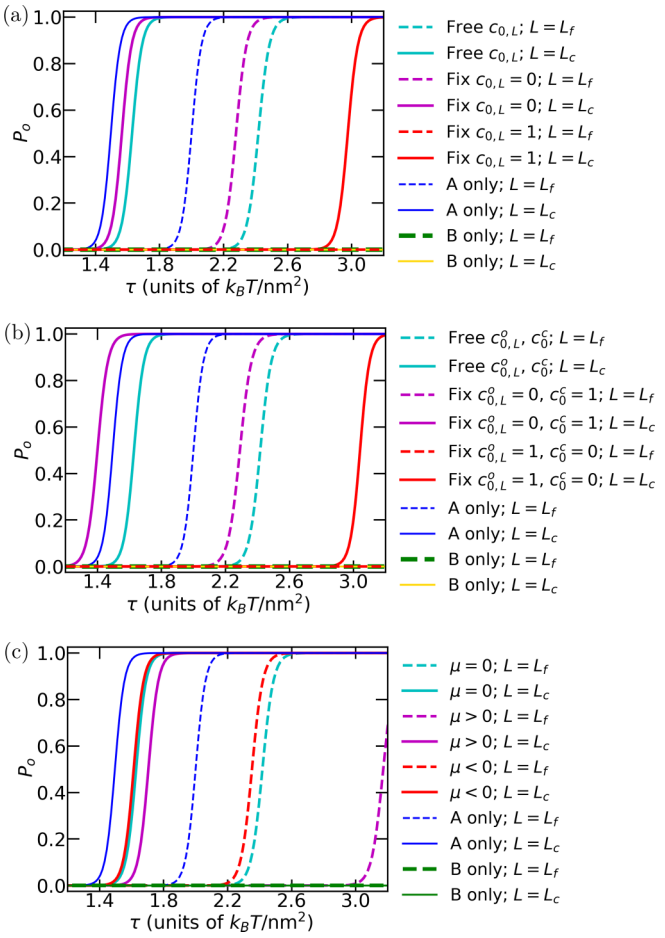

FIG. 9. Cooperativity in the tension-dependent gating of MscL in heterogeneous bilayers. Probability that the MscL protein at the center of the membrane patch is in its open state, P_o in Eq. (9), vs membrane tension τ for (a) identical fixed-value boundary conditions on c at all bilayer-protein interfaces with $\mu = 0$, (b) the indicated fixed-value boundary conditions on c at $r = R$ and $r = R + L$ in the closed (c_0^c) and open ($c_{0,L}^o$) conformational states of MscL with $\mu = 0$, and (c) natural boundary conditions on c at all bilayer-protein interfaces with $\mu = \pm 10^{-2}\ k_BT/\text{nm}^2$ ($\mu \gtrless 0$). For reference, we also show in all three panels the corresponding MscL gating curves obtained with natural boundary conditions on c at all bilayer-protein interfaces with $\mu = 0$, as well as the corresponding MscL gating curves obtained for homogeneous bilayers composed solely of lipid species A or B [38]. We use $H_0 = H^c$ and $H_0 = H^o$ for the closed and open conformational states of the MscL protein at the center of the membrane patch, and $H_L = H^o$ for the proteins at the outer membrane patch boundary. The edge-to-edge protein separations considered here, $L = L_c = 3$ nm and $L = L_f = 12$ nm, correspond to regimes with strong and weak bilayer-mediated protein interactions (see also Figs. 7 and 8).

same lipid affinity in its closed and open states [see Fig. 9(a)]. We first note [38] that, for heterogeneous bilayers with natural boundary conditions on c at the bilayer-protein interfaces, the MscL gating tension decreases as L is decreased, $\bar{\tau}_c < \bar{\tau}_f$, with amplified MscL cooperativity as compared to homogeneous bilayers. Figure 9(a) shows that a lipid-MscL chemical affinity can also yield amplified MscL cooperativity with $\bar{\tau}_c < \bar{\tau}_f$, resulting in substantial shifts in the MscL gating tension as L is decreased. Interestingly, we find in Fig. 9(a) that, if MscL has an affinity for lipid species B in its closed and open states, the (hypothetical) MscL gating tension is greater than the approximate bilayer rupture tension $\tau_r \approx 3\ k_BT/\text{nm}^2$ [54] for $L = L_f$, $\bar{\tau}_f > \tau_r$, but $\bar{\tau}_c < \tau_r$ for $L = L_c$. Thus, for these boundary conditions on c, MscL gating relies on cooperative effects. Allowing for distinct lipid-MscL affinities in the closed and open conformational states of MscL further broadens the cooperative response of MscL to changes in membrane tension [see Fig. 9(b)], and can further amplify cooperative shifts in the MscL gating tension.

In addition to lipid-protein chemical affinity, a nonzero chemical potential can also substantially affect protein cooperativity in heterogeneous bilayers [see Fig. 9(c)]. For instance, using natural boundary conditions on c in the closed and open states of MscL, cooperativity in MscL gating is markedly amplified for $\mu > 0$ in Fig. 9(c) as compared to $\mu = 0$. This can be understood intuitively by noting that $\mu > 0$ biases the lipid bilayer composition towards lipid species B, which tends to produce a strongly increased bilayer thickness deformation energy for the open state of MscL, thus increasing the significance of cooperative effects with respect to scenarios with $\mu = 0$. In contrast, $\mu < 0$ in Fig. 9(c) produces only comparatively modest shifts in the MscL gating cooperativity with respect to $\mu = 0$. Similarly as in Figs. 9(a) and 9(b), cooperative effects are needed in Fig. 9(c) for $\mu > 0$ to shift the MscL gating tension to values smaller than the bilayer rupture tension τ_r. Taken together, the results in Fig. 9 thus show that a lipid-protein chemical affinity or a nonzero lipid chemical potential can substantially affect protein cooperativity in heterogeneous lipid bilayers and, in particular, amplify cooperative effects.

V. SUMMARY AND CONCLUSIONS

Cell membranes are composed of a great variety of protein and lipid species with distinct unperturbed hydrophobic thicknesses, and show an intricate submicron organization of lipids and proteins into domains with defined composition [1–4,17,18]. A wide range of experiments suggest that membrane hydrophobic thickness provides a key control parameter for cell membrane organization [1–3,55–57]. To achieve hydrophobic matching, the lipid bilayer tends to deform around membrane proteins so as to match the protein hydrophobic thickness at bilayer-protein interfaces [15–18]. Such protein-induced distortions of the lipid bilayer hydrophobic thickness incur a substantial energy cost that depends critically on the hydrophobic mismatch between the membrane protein and the lipids localized around the membrane protein. We have combined here the membrane elasticity theory of protein-induced lipid bilayer thickness deformations with the LG theory of lipid domain formation to systematically explore the mechanochemical coupling of lipid organization and protein function through membrane thickness deformations.

Protein-induced lipid bilayer thickness deformations are localized over a scale of approximately 4 nm about membrane proteins [15–17,22,24–28,44,54], which corresponds to roughly one-half the typical protein-protein separation in cell membranes [4,18]. The resulting overlap in protein-induced

bilayer thickness deformations gives rise to bilayer-thickness-mediated protein interactions that, at small enough protein separations, tend to be strongly favorable for proteins with identical hydrophobic thickness [16,24–28,33,35] and have been observed to yield protein aggregation in membranes [29–32,34,36]. Furthermore, protein-induced lipid bilayer thickness deformations induce a coupling of protein conformational state and lipid bilayer thickness, which provides a general mechanism for protein regulation through lipid bilayer mechanics [15,17–23,44]. For membrane proteins at close enough separations, the combination of bilayer-thickness-mediated protein interactions and the coupling of protein conformational state to lipid bilayer thickness is expected to produce cooperativity in membrane protein function [18,25–27,32,33,35,36]. We have extended here the classic theory of bilayer-thickness-mediated protein interactions and protein cooperativity [16,24–28,33,35] to account for heterogeneous lipid bilayers composed of two lipid species with distinct unperturbed hydrophobic thicknesses. We find that lipid heterogeneity can yield colocalization of lipids and membrane proteins according to their preferred hydrophobic thickness, and can have intricate effects on membrane protein regulation, protein clustering, and protein cooperativity driven by bilayer thickness deformations.

For small membrane gradients in homogeneous lipid bilayers, bilayer thickness and bilayer midplane deformations decouple to leading order [44,70]. But, similarly as for thickness deformations, midplane deformations in heterogeneous lipid bilayers couple to the lipid bilayer composition [41–43]. Interestingly this means that, even for small membrane gradients, heterogeneity in lipid composition couples bilayer thickness and bilayer midplane deformations. Depending on the specific scenario considered, bilayer thickness and bilayer midplane deformations may thus be competing with each other in driving lipid organization. For MscL, experiments and theory suggest that bilayer thickness deformations are dominant with only weak bilayer midplane deformations [21,22,44]. We therefore expect that, in general, the bilayer midplane deformations induced by MscL would not alter the behavior described here. A caveat is that, for lipid bilayers with large intrinsic curvature, even an approximately flat bilayer-protein interface may produce pronounced membrane curvature deformations. In this case, bilayer midplane deformations could have a substantial effect on membrane organization even if the protein has an approximately cylindrical shape.

Building on a previous short communication [38], we considered here a purely mechanical coupling of lipid and protein composition through the energetics of protein-induced lipid bilayer thickness deformations as well as a chemical coupling driven by preferential interactions between particular lipid and protein species [58–65]. In general, both types of lipid-protein coupling are expected to occur in cell membranes. A chemical affinity between particular lipid and protein species could also be engineered synthetically. Our results show how the local lipid composition around membrane proteins depends on the protein hydrophobic thickness, the lipid-protein chemical affinity, and the local lipid chemical potential. Employing MscL as a model system [9,21,22,54], we find that the resultant lipid-protein organization can induce transitions in the protein conformational state. We thereby focused on lipid bilayer configurations that correspond to global energy minima of the bilayer energy. In addition to these global energy minima, we also found numerically local energy minima that correspond to metastable states of the bilayer-protein system. Interestingly, when considering transitions in the protein conformational state, such metastable states may give rise, in addition to internal protein degrees of freedom [22], to short-lived substates of the bilayer-protein system.

Our calculations show that lipid heterogeneity can yield substantial modifications of bilayer-thickness-mediated protein interactions. Notably, we find that lipid heterogeneity can expand the range of attractive protein interactions and amplify membrane protein cooperativity. In the case of MscL, for instance, this amplification of protein cooperativity manifests itself as pronounced shifts in the MscL gating tension. The predicted effects of lipid heterogeneity on MscL gating could, perhaps, be tested most directly in experiments by measuring MscL gating curves for bilayer vesicles with heterogeneous, rather than homogeneous, lipid compositions [21]. The predicted effects of bilayer thickness deformations on lipid and protein organization, and on bilayer-mediated protein interactions, could be tested experimentally by, for instance, measuring the spatial distributions of lipids and proteins in heterogeneous bilayers [29–32,34,36]. Taken together, our results suggest that membrane thickness deformations provide a physical mechanism for the formation of membrane domains with controlled mechanical properties that, in turn, can affect the membrane protein conformational state. The coupling of protein-induced bilayer thickness deformations [15–17,24–28,44] and lipid domain formation [41,45–53] may provide a general physical mechanism underlying the observed supramolecular organization of cell membranes [1–4].

ACKNOWLEDGMENTS

This work was supported at USC by NSF Grants No. DMR-2051681, No. PHY-1806381, and No. DMR-1554716, and the USC Center for Advanced Research Computing. At KITP, this research was supported in part by NSF Grant No. NSF PHY-1748958, NIH Grant No. R25GM067110, and the Gordon and Betty Moore Foundation Grant No. 2919.02.

APPENDIX A: ONE-DIMENSIONAL MODEL

Previous work [16,24–28] has shown that generic properties of bilayer-thickness-mediated protein interactions in homogeneous lipid bilayers—such as the order of magnitude, sign, and approximate range of bilayer-mediated protein interactions—are already captured by a highly simplified model in which the membrane is described as an effectively one-dimensional (1D) system. Such a 1D approach also successfully captures basic properties of the tension-dependent gating of MscL [22,54]. In this Appendix we generalize this approach to protein-induced bilayer thickness deformations in heterogeneous lipid bilayers composed of two lipid species with distinct unperturbed hydrophobic thicknesses, and thereby complement the axisymmetric, two-dimensional (2D) model developed in Sec. II.

In analogy to the 2D system in Sec. II, we take our 1D system to have a lateral extent L, as measured from the edge of the protein to the system boundary. We approximate the total bilayer energy by the integral over the 1D energy density $g^{(1D)}(x)$ multiplied by the circumference of the protein at the center of the membrane patch, $2\pi R$:

$$G^{(1D)} = 2\pi R \int_0^L g^{(1D)}(x)\, dx, \tag{A1}$$

where the 1D energy density is given by

$$\begin{aligned} g^{(1D)}(x) = {} & \frac{K_b}{2}\left(\frac{d^2h}{dx^2}\right)^2 + \frac{K_t}{2}\left(\frac{h-a(c)}{a(c)}\right)^2 + \frac{\tau}{2}\left(\frac{dh}{dx}\right)^2 \\ & + \tau\left(\frac{h-a(c)}{a(c)}\right) + \frac{\tau^2}{2K_t} + \frac{\varepsilon}{2}\left(\frac{dc}{dx}\right)^2 \\ & + b_0 - \frac{b_1}{2}\left(c-\frac{1}{2}\right)^2 + \frac{b_2}{4}\left(c-\frac{1}{2}\right)^4 \\ & - \mu c + \mu_0, \end{aligned} \tag{A2}$$

with the 1D scalar functions $h(x)$ and $c(x)$. As in Eq. (4) in Sec. II, we assume that the unperturbed bilayer leaflet thickness, $a(c)$, is a linear function of the lipid composition [see Eq. (5)], while K_b and K_t are constants. Similarly as in Sec. II, we minimize the energy functional in Eq. (A1) subject to natural (free) or fixed-value boundary conditions on $h(x)$, dh/dx, and $c(x)$ [75,76], using the L-BFGS-B solver [73,74]. In particular, the 1D natural boundary conditions are given by

$$\left[\frac{d}{dx}\left(\tau h - K_b\frac{d^2h}{dx^2}\right)\right]_{x=x_b} = 0, \tag{A3a}$$

$$\left.\frac{d^2h}{dx^2}\right|_{x=x_b} = 0, \tag{A3b}$$

$$\left.\frac{dc}{dx}\right|_{x=x_b} = 0 \tag{A3c}$$

with $x_b = 0$ or $x_b = L$. The corresponding 1D fixed-value boundary conditions are given by

$$h(x_b) = H_b, \tag{A4a}$$

$$\left.\frac{dh}{dx}\right|_{x=x_b} = s_b, \tag{A4b}$$

$$c(x_b) = c_b \tag{A4c}$$

with $x_b = 0$ or $x_b = L$, where H_b, s_b, and c_b take given, fixed values (see Sec. II). Similarly as for the 2D model developed in Sec. II, we use here Eq. (A4b) with $s_b = 0$ throughout.

The 1D model in Eqs. (A1) and (A2) is not expected to yield precise estimates of the numerical values of the bilayer energy G. For instance, the magnitude of G as a function of protein hydrophobic thickness tends to be larger for the 2D model than for the 1D model [see Fig. 10(a)]. Similarly, we also find shifts in the predicted bilayer-mediated protein interactions [see Fig. 10(b)] as well as in the predicted MscL gating tensions in the noninteracting and interacting regimes [see Fig. 10(c)]. But, consistent with previous work on protein-induced bilayer thickness deformations in homogeneous bilayers [16,22,24,54], we find that Eqs. (A1) and (A2)

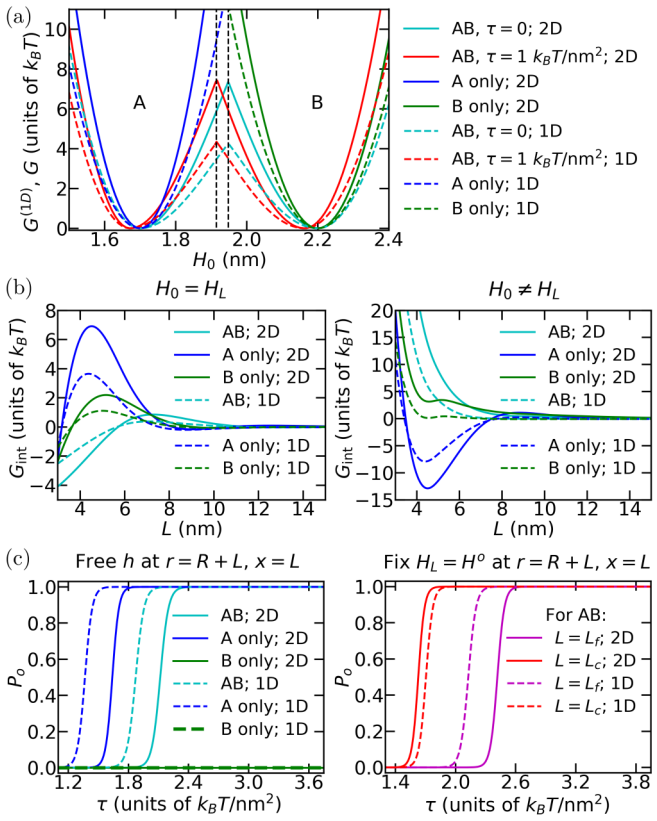

FIG. 10. Comparing 1D and 2D model results. (a) Total 1D bilayer energy $G^{(1D)}$ in Eq. (A1) and total 2D bilayer energy G in Eq. (4) as a function of H_0 with $R = R^c$ for a heterogeneous bilayer containing lipid species A and B (AB) at $\tau = 0$ and $\tau = 1\ k_BT/\text{nm}^2$, and for homogeneous bilayers composed solely of lipid species A or B at $\tau = 0$. The dashed vertical lines indicate $H_0 = H_0^*$, where the dominant lipid composition in the bilayer patch changes from lipid species A to lipid species B, for $\tau = 0$ and $\tau = 1\ k_BT/\text{nm}^2$ (right to left). The 1D and 2D values of H_0^* are identical within numerical accuracy. We set $L = 20$ nm. (b) Bilayer-mediated protein interactions $G_{\rm int}$ as a function of L at $\tau = 0$ for proteins with identical hydrophobic thickness $H_0 = H_L = 2.0$ nm (left panel) and distinct hydrophobic thicknesses $H_0 = 2.2$ nm and $H_L = H^o$ (right panel) obtained from the 1D and 2D models for heterogeneous and homogeneous lipid bilayers. To calculate $G_{\rm int}(L)$, we subtracted from the total 1D bilayer energy $G^{(1D)}$ in Eq. (A1) and the total 2D bilayer energy G in Eq. (4) the respective values of $G^{(1D)}$ and G obtained in the large-L, noninteracting regimes (see also Appendix E). (c) MscL gating probability P_o in Eq. (9) as a function of τ with natural boundary conditions on h at the outer membrane patch boundary for $L = 20$ nm (left panel), and with the fixed-value boundary condition $H_L = H^o$ at the outer membrane patch boundary for $L = L_f = 12$ nm and $L = L_c = 3$ nm (right panel). We used Eq. (A4b) with $s_b = 0$ and $\mu = 0$ throughout. Unless indicated otherwise, we employed natural boundary conditions for h and c.

do capture important generic features of lipid-protein interactions in heterogeneous bilayers. In particular, we find that most of the conclusions we arrived at in this article based on the 2D model in Eqs. (1) and (2), which do not rely on the precise numerical values of G, remain unchanged if Eqs. (1) and (2) are replaced by Eqs. (A1) and (A2). Broadly speaking, the main difference between our 1D and 2D results

is that the predicted effects of lipid bilayer heterogeneity on lipid-protein organization and regulation through membrane thickness deformations tend to be more pronounced in the 2D model than in the (less accurate) 1D model.

APPENDIX B: ANALYTIC SOLUTION FROM A VARIATIONAL APPROACH

In this Appendix we adapt the variational approach described in Ref. [54] to find approximate, analytic solutions for the leaflet thickness field h and the bilayer composition field c. For simplicity, we thereby focus on the 1D model described in Appendix A. Specifically, we consider the 1D bilayer energy given by Eqs. (A1) with (A2) at zero membrane tension, $\tau = 0$, and zero chemical potential, $\mu = 0$. For $h(x)$, we use the fixed-value boundary conditions in Eqs. (A4a) and (A4b) with $s_b = 0$ at the bilayer-protein interface, $x = 0$, and the natural boundary conditions in Eqs. (A3b) and (A3a) at the outer edge of the membrane patch, $x = L$. For $c(x)$, we use the natural boundary condition in Eq. (A3c) at both domain boundaries. We focus on the limit of an infinitely large membrane patch, $L \to \infty$. This scenario corresponds to bilayer-protein interactions for dilute protein concentrations in the membrane with no specific lipid-protein affinities, but an analogous variational approach could be developed for membranes crowded with proteins or if there are preferential chemical interactions between particular lipid and protein species.

For our variational ansatz, we consider trial functions of the form

$$h(x) = h_d\left(1 + \frac{x}{\lambda_d}\right)e^{-x/\lambda_d} + h_\infty, \tag{B1}$$

$$c(x) = \begin{cases} c_d\left(1 + \frac{x}{\lambda_d}\right)e^{-x/\lambda_d} + c_\infty & \text{if } a(0) \leqslant H_0 \leqslant a(1), \\ c_\infty & \text{otherwise,} \end{cases} \tag{B2}$$

where λ_d is the decay length of the thickness and composition profiles, and $h_d = H_0 - h_\infty$ and $c_d = c(0) - c_\infty$ are the differences between the respective values of h and c at $x = 0$ and $x \to \infty$. Based on the results in the main text, we assume in Eq. (B2) that the lipid composition of the membrane patch under consideration is homogeneous for values of H_0 outside the range $a(0) \leqslant H_0 \leqslant a(1)$. For the bilayer energy $G^{(1D)}$ in Eq. (A1) to be finite we must have $g^{(1D)}(x) \to 0$ in Eq. (A2) as $x \to \infty$. We thus assume that either $c_\infty = 0$ or $c_\infty = 1$, and $h_\infty = \alpha_1 c_\infty + \alpha_0$. We focus here on bilayers composed of lipid species A and B, in which case $\alpha_1 = 0.5$ nm and $\alpha_0 = 1.7$ nm [see Eq. (5)].

We regard the parameters λ_d, c_d, and $c_\infty = 0, 1$ in the ansatz solutions in Eqs. (B1) and (B2) as free parameters with respect to which the bilayer energy in Eq. (A1) with Eq. (A2) must be minimized [54]. To this end, we substitute the trial functions in Eqs. (B1) and (B2) into Eq. (A2). Assuming small h_d and c_d such that $|h_d/h_\infty| \ll 1$ and $|c_d| \ll 1$, we then expand Eq. (A2) up to second order in h_d and c_d to obtain the following approximate form of the bilayer energy in Eq. (A1):

$$G^{(1D)}(\lambda_d, c_d) \approx \frac{\pi R}{4\lambda_d^3}\left[\left(\frac{5K_t}{h_\infty^2}(h_d - \alpha_1 c_d)^2 + 10 b_1 c_d^2\right)\lambda_d^4 + \varepsilon c_d^2 \lambda_d^2 + K_b h_d^2\right], \tag{B3}$$

which depends on c_∞ through h_∞ and h_d. Note that, upon setting $c_d = 0$, we recover from Eq. (B3) the variational expression for the 1D energy of a homogeneous bilayer at $\tau = 0$ in Ref. [54], which is also equivalent to Eq. (A1) with Eqs. (A2), (B1), and (B2) for $H_0 \leqslant a(0)$ or $H_0 \geqslant a(1)$. We allow for both $c_\infty = 0$ and $c_\infty = 1$, and choose the value of c_∞ yielding the smaller value of $G^{(1D)}$ in Eq. (B3). To minimize Eq. (B3) with respect to λ_d and c_d we solve

$$\frac{\partial G^{(1D)}}{\partial \lambda_d} = 0, \tag{B4}$$

$$\frac{\partial G^{(1D)}}{\partial c_d} = 0. \tag{B5}$$

In particular, from Eq. (B5) it follows that

$$c_d = \frac{5\alpha_1 K_t \lambda_d^2 h_d}{(5\alpha_1^2 K_t + 10 b_1 h_\infty^2)\lambda_d^2 + \varepsilon h_\infty^2}. \tag{B6}$$

By combining Eq. (B4) with Eq. (B6) and setting $\Lambda = \lambda_d^2$, we arrive at the quartic equation,

$$\Lambda^4 + \frac{\varepsilon}{5}\left(1 - \frac{15\alpha_1^2 K_t}{2W_0}\right)\Lambda^3 + \frac{\varepsilon^2 h_\infty^2}{10 W_0}\left(1 - \frac{3W_0^2 K_b}{5h_\infty^3 K_t}\right)\Lambda^2 - \frac{3\varepsilon h_\infty^2 K_b}{25 K_t}\Lambda - \frac{3\varepsilon^2 h_\infty^4 K_b}{50 W_0 K_t} = 0, \tag{B7}$$

where $W_0 = 5(2b_1 h_\infty^2 + \alpha_1^2 K_t)$, which we solve analytically for λ_d.

Note from Eq. (B6) that c_d is directly proportional to h_d, and from Eq. (B7) that λ_d only depends on the constants K_b, K_t, ε, b_1, α_1 and h_∞. Upon substitution of c_d in Eq. (B6) into Eq. (B3) we thus find $G^{(1D)} \sim h_d^2$ for $|h_d/h_\infty| \ll 1$. Hence, the bilayer energy shows a quadratic dependence on protein hydrophobic thickness around $H_0 = h_\infty$, with $h_\infty = 1.7$ nm or $h_\infty = 2.2$ nm for a bilayer at $\tau = 0$ composed of lipid species A and B. As illustrated in Fig. 11(a), this scaling behavior is consistent with the numerically calculated $G^{(1D)}(H_0)$. Note that, near the minima of $G^{(1D)}(H_0)$, $G^{(1D)} \sim h_d^2$ on both the left and right sides of the minima but with, in general, different prefactors [see also Eq. (B2)]. Figures 11(b) and 11(c) illustrate that, for $a(0) \leqslant H_0 \leqslant a(1)$ with $|h_d/h_\infty| \ll 1$ and $|c_d| \ll 1$, the ansatz solutions in Eqs. (B1) and (B2) yield quite good agreement with the corresponding numerical solutions for the 1D leaflet thickness and bilayer composition fields, as well as for the bilayer energies. In particular, if $h_\infty = 2.2$ nm, $c_\infty = 1$, and $|h_d| \lessapprox 0.1$ nm, the percentage differences between the ansatz and numerical solutions for $h(x)$ and $c(x)$ are less than 2%, and the bilayer energies agree to within approximately 10%. More accurate variational results could be obtained by including higher-order terms in Eq. (B3) and by allowing for different, more complicated, forms of the ansatz solutions.

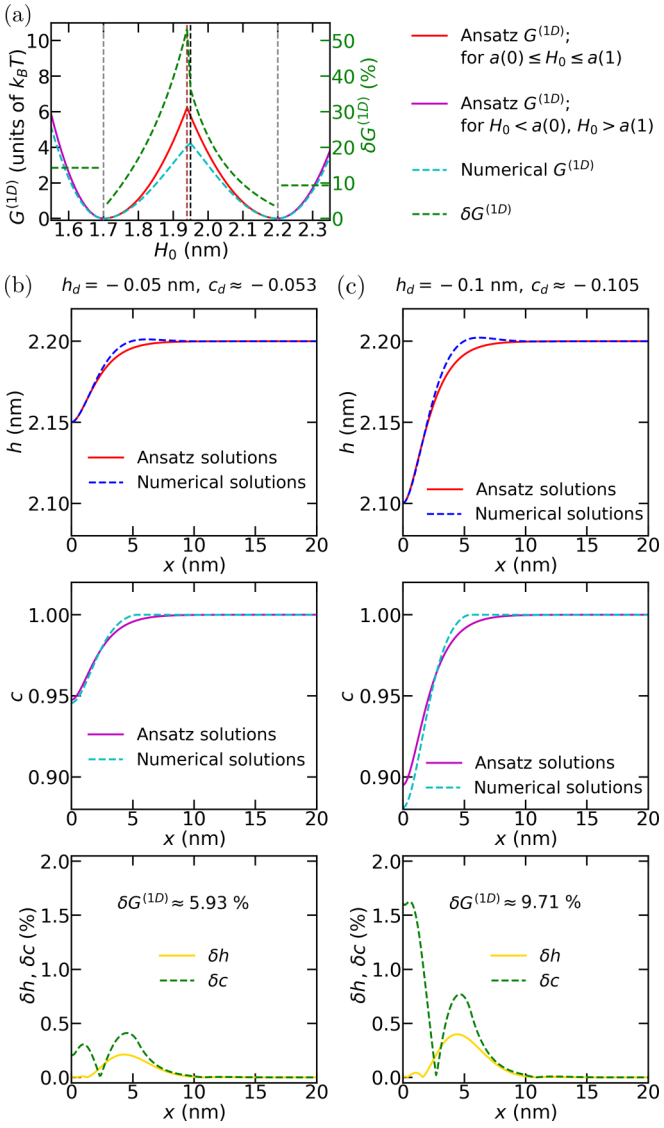

FIG. 11. Comparing ansatz and numerical solutions. (a) Bilayer energy $G^{(1D)}$ as a function of H_0 for the ansatz solution in Eq. (B3) and corresponding numerical solutions, and absolute percentage difference between the ansatz and numerical solutions, $\delta G^{(1D)}$. The brown and black dashed vertical lines indicate the points at which the dominant lipid composition in the bilayer changes for the ansatz and numerical solutions, respectively, while the gray dashed vertical lines indicate the (identical) minima of the ansatz and numerical solutions. (b) 1D leaflet thickness fields h for the ansatz solution in Eq. (B1) with the corresponding numerical solutions (top panels), 1D bilayer composition fields c for the ansatz solution in Eq. (B2) with the corresponding numerical solutions (middle panels), and absolute percentage differences δh and δc between the ansatz and numerical solutions (bottom panels) as a function of x. We have $c_\infty = 1$ and $h_\infty = 2.2$ nm, with $H_0 = 2.15$ nm so that $h_d = -0.05$ nm (left panels) and with $H_0 = 2.10$ nm so that $h_d = -0.1$ nm (right panels). Analytic solution of Eqs. (B4) and (B5) yields $\lambda_d \approx 1.21$ nm and the indicated values of c_d. For all panels, we used for h the fixed-value boundary conditions in Eqs. (A4a) and (A4b) at $x = 0$ and the natural boundary conditions in Eqs. (A3b) and (A3a) at $x = L$, with the natural boundary condition in Eq. (A3c) for c at $x = 0$ and $x = L$. We set $R = 2.5$ nm, $\tau = 0$, and $\mu = 0$ for all panels. We obtained the numerical solutions as described in Appendix A with $L = 20$ nm.

APPENDIX C: DEPENDENCE OF BILAYER BENDING RIGIDITY AND THICKNESS DEFORMATION MODULUS ON LIPID COMPOSITION

The purpose of this Appendix is to examine the relative importance of the dependence of K_b, K_t, and a in Eq. (1) on lipid composition [12,17,18,44] for lipid-protein organization and regulation through membrane thickness deformations. In analogy to $a(c)$ in Eq. (5) we assume, based on the data in Ref. [12], that $K_b(c)$ and $K_t(c)$ can be approximated by linear functions of c,

$$K_b(c) \approx \beta_1 c + \beta_0, \tag{C1}$$

where $\beta_1 = 15\ k_BT$ and $\beta_0 = 14\ k_BT$ such that $K_b(0) \approx 14\ k_BT$ and $K_b(1) \approx 29\ k_BT$ [12,44], and

$$K_t(c) \approx \gamma_1 c + \gamma_0, \tag{C2}$$

where $\gamma_1 = 5\ k_BT/\text{nm}^2$ and $\gamma_0 = 58\ k_BT/\text{nm}^2$ such that $K_t(0) \approx 58\ k_BT/\text{nm}^2$ and $K_t(1) \approx 63\ k_BT/\text{nm}^2$ [12,44].

In Fig. 12(a) we illustrate the effect of the dependence of K_b and K_t on c in Eqs. (C1) and (C2) on the total bilayer energy in Eq. (4) for a single-membrane protein. Figure 12(a) suggests that variations in $K_b(c)$ or $K_t(c)$ only produce minor shifts in the energy landscape of bilayer-protein interactions in heterogeneous bilayers. To further quantify the ramifications of a dependence of K_b or K_t on c we consider the percentage difference between the total bilayer energy obtained with constant K_b and K_t as described in Sec. II, G, and the corresponding total bilayer energy obtained with the expressions for $K_b(c)$ and $K_t(c)$ in Eqs. (C1) and (C2), $\bar{G}$,

$$\delta = 100 \times \left| \frac{G - \bar{G}}{G} \right|. \tag{C3}$$

Figures 12(b) and 12(c) show Eq. (C3) for selected scenarios corresponding to noninteracting and interacting membrane proteins in heterogeneous bilayers. We find $\delta < 20\%$ in Figs. 12(b) and 12(c), with $\delta < 10\%$ for many of the scenarios considered here.

APPENDIX D: ENERGY MINIMIZATION

We employ [38] the L-BFGS-B solver [74]—a low memory (L) version of the Broyden-Fletcher-Goldfarb-Shanno (BFGS) algorithm [73] with bounded (B) constraints—to directly minimize the functional G in Eq. (4) and thus to numerically find $h(r)$ and $c(r)$. Numerical minimization methods that implement this solver were also used in previous work on bilayer-thickness-mediated protein interactions [28]. The L-BFGS-B solver aims to find a local minimum of a given functional $\mathcal{G}[v]$ with respect to a function $v(t)$. We discretize the energy functional in Eq. (6) with coordinates $r \to r - R$ using finite differences [81]. The discretized function $v(t_i) \to v_i$ thereby becomes the ith entry of the input vector $\vec{v}$. Since we have two functions $h(r)$ and $c(r)$ in the model in Sec. II, we consider a vector $\vec{v}$ of length N partitioned into two domains of length $n = N/2$, $(v_0, \ldots, v_{n-1}, v_n, \ldots, v_{N-1}) = (h_0, .., h_{n-1}, c_0, \ldots, c_{n-1})$. We discretize the integral in Eq. (6) as a sum over grid points with lattice spacing $\Delta r = L/(n-1)$. Starting from a given initial value of the input vector $\vec{v}_0$, the L-BFGS-B solver iteratively finds better

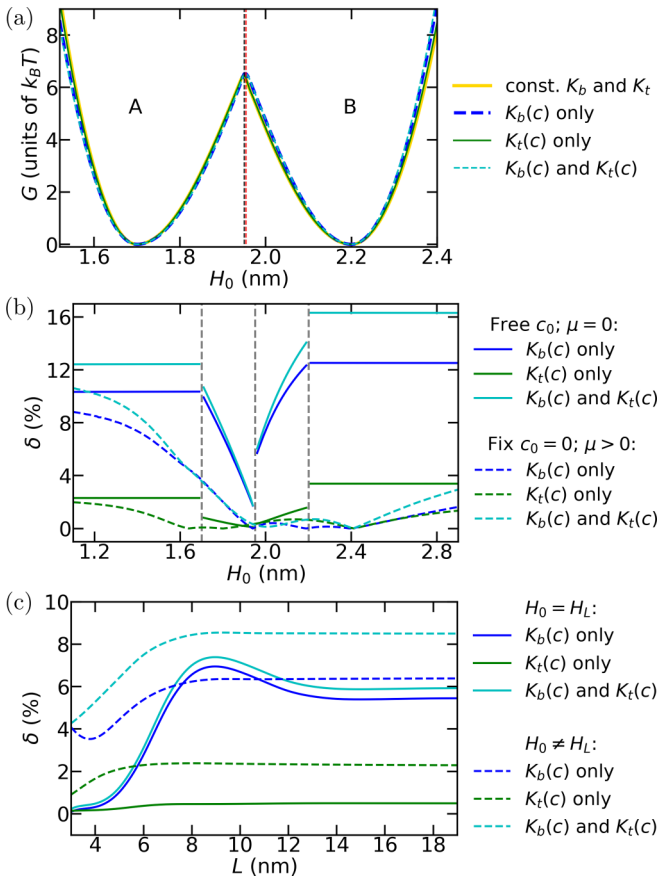

FIG. 12. Total bilayer energy with c-dependent K_b or K_t. (a) Bilayer energy G in Eq. (4) for a single-membrane protein as a function of protein hydrophobic thickness H_0 with the expressions for $K_b(c)$ and $K_t(c)$ in Eqs. (C1) and (C2), as well as the constant $K_b = 20\ k_BT$ and $K_t = 60\ k_BT/\text{nm}^2$ [12,18] considered in the remainder of this article. The dashed vertical lines show $H_0 = H_0^*$, where the dominant lipid composition in the membrane patch changes from lipid species A to lipid species B. For constant K_b and K_t we have $H_0^* \approx 1.950$ nm (black dashed line), and with the c-dependent K_b and K_t in Eqs. (C1) and (C2) we find $H_0^* \approx 1.954$ nm (red dashed line). We set $L = 20$ nm. (b, c) Percentage difference between the total bilayer energy G in Eq. (4) obtained with constant K_b and K_t as described in Sec. II, and the corresponding total bilayer energy obtained with the expressions for $K_b(c)$ or $K_t(c)$ in Eqs. (C1) and (C2), δ in Eq. (C3), for noninteracting [panel (b)] and interacting [panel (c)] membrane proteins in heterogeneous bilayers. In panel (b) we used $\mu = 10^{-2}\ k_BT/\text{nm}^2$ for $\mu > 0$ and set $L = 20$ nm. In panel (c) we used $H_0 = H_L = 2.0$ nm for $H_0 = H_L$, and $H_0 = 2.2$ nm and $H_L = 1.3$ nm for $H_0 \neq H_L$. In all panels we set, unless specified otherwise, $\mu = 0$ and used natural boundary conditions on h, ∇h, and c. We set $\tau = 0$ and employed $a(c)$ in Eq. (5).

estimates of $\vec{v}$ so as to minimize $\mathcal{G}$. To this end, the L-BFGS-B solver employs a steepest-decent method based on the discretized energy functional $\vec{\nabla}\mathcal{G}$ with entries given by $\nabla\mathcal{G}_i = \partial G/\partial v_i$ [73,74]. Unless mandated by fixed-value boundary conditions, we do not restrict the h_i variables in $\vec{v}$. We always restrict the c_i variables in $\vec{v}$ to the range $0 \leqslant c_i \leqslant 1$.

A complication arises here in that the derivatives in Eq. (4) can yield exterior "ghost" points lying outside the grid used for the numerical minimization procedure. We determine the values of v_i at these exterior points from the boundary conditions on the h and c fields. For instance, employing the forward and central discretizations [81] for the first and second derivatives of h with respect to r, we obtain the following expression for the discretized Laplacian of h:

$$(\nabla^2 h)_i = \frac{(1+w_i)h_{i+1} - (2+w_i)h_i + h_{i-1}}{(\Delta r)^2}, \tag{D1}$$

where $w_i = \Delta r/(R + i\Delta r)$. Evaluating Eq. (D1) at the boundaries with $i = 0$ and $i = n-1$, gives two undefined exterior values, h_{-1} and h_n. If, for instance, natural boundary conditions are imposed on h at the system boundaries, h_{-1} and h_n are specified by Eq. (7a), which gives

$$(1+w_0)h_1 - (2+w_0)h_0 + h_{-1} = 0, \tag{D2a}$$

$$(1+w_{n-1})h_n - (2+w_{n-1})h_{n-1} + h_{n-2} = 0. \tag{D2b}$$

Similarly, if fixed-value boundary conditions are imposed on h at the system boundaries, h_{-1} and h_n are specified by Eq. (8a), which gives

$$h_0 - h_{-1} = 0, \tag{D3a}$$

$$h_n - h_{n-1} = 0. \tag{D3b}$$

Analogous considerations apply to all combinations of boundary conditions considered here.

The L-BFGS-B solver employed here gives a local energy minimum near the initial values of the input vector $\vec{v}$ that, in principle, may not correspond to the global energy minimum of the system. We address this issue through the multistart method [83,84], which provides a simple approach for determining a global minimum within a bounded range through a local-minimum solver. We thereby test different initial values for $\vec{v}$ corresponding to $0 \leqslant c \leqslant 1$ using increments of 0.1, with $h = a(c)$. For the boundary conditions and system sizes considered here, we generally find distinct local energy minima with the initial trial values $c = 0$ and $c = 1$. We also find that, for protein hydrophobic thicknesses $H_0 \approx 1.95$ nm, a third local energy minimum may appear for the initial trial value $c = 0.5$. From the sets of local energy minima determined through the L-BFGS-B solver with the multistart method, we take the solutions with the smallest energy to correspond to the global energy minima.

It is instructive to compare the results obtained through direct numerical minimization of Eq. (4) with the corresponding solutions of the Euler-Lagrange equations associated with Eq. (4), which follow from the calculus of variations [75,76]:

$$K_b\nabla^4 h - \tau\nabla^2 h + \frac{K_t}{a(c)^2}[h - a(c)] + \frac{\tau}{a(c)} = 0, \tag{D4}$$

$$\mu - \varepsilon\nabla^2 c - b_1(c - c_0) + b_2(c - c_0)^3 - \frac{K_t}{a(c)^3}h[h - a(c)]a'(c) - \frac{\tau}{a(c)^2}a'(c)h = 0. \tag{D5}$$

For the parameter values used here, Eqs. (D4) and (D5) can be conveniently solved using the *NDSolve*-command in *Mathematica* [82] subject to the boundary conditions in Eqs. (7a)–(7c) or Eqs. (8a)–(8c), provided that L is small enough with $L \lesssim 5$ nm and that ε in Eq. (2) is increased from the value $\varepsilon = 1\ k_BT$, employed in the remainder of this

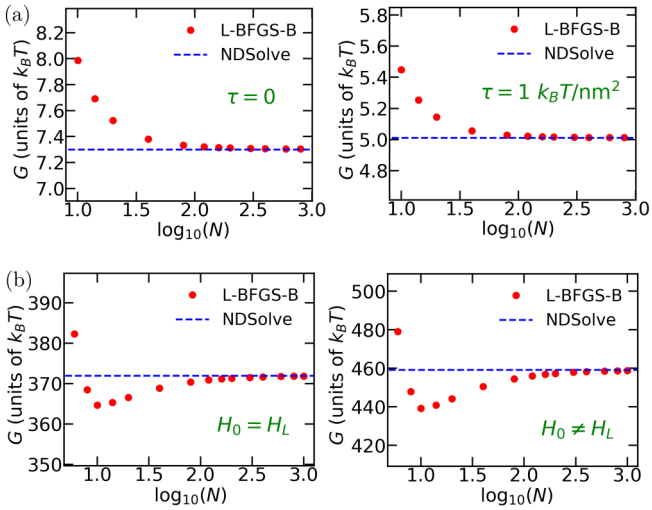

FIG. 13. Convergence tests for the total bilayer energy G in Eq. (4) for membrane proteins in heterogeneous bilayers. We consider here (a) single proteins with $H_0 = 2.0$ nm at $\tau = 0$ (left panel) and $\tau = 1\ k_BT/\text{nm}^2$ (right panel) and (b) interacting proteins with identical hydrophobic thickness ($H_0 = H_L = 2.0$ nm; left panel) and distinct hydrophobic thickness ($H_0 = 2.2$ nm and $H_L = 1.3$ nm; right panel) with $c_0 = 1$ and $c_L = 0$. Results obtained using the L-BFGS-B solver with the multistart method are indicated by red data points and plotted as a function of the logarithm (base 10) of the number of grid points used in the L-BFGS-B solver, $\log_{10}(N)$. For comparison, we also show the corresponding results obtained by numerically solving the Euler-Lagrange equations in Eqs. (D4) and (D5) using the NDSolve command in *Mathematica* [82] (dashed blue horizontal lines). We set here $\varepsilon = 100\ k_BT$, $\mu = 0$, $R = 3$ nm, and $L = 5$ nm for all panels and used, unless specified otherwise, natural boundary conditions on h, ∇h, and c.

article, to $\varepsilon \gtrapprox 100\ k_BT$. As illustrated in Fig. 13, the results obtained through direct numerical minimization of Eq. (4) via the L-BFGS-B solver with the multistart method agree with the corresponding results obtained by numerically solving Eqs. (D4) and (D5), provided that the number of grid points used for the L-BFGS-B solver, N, is large enough. Unless specified otherwise we used, throughout this article, $N \approx 500$ in the L-BFGS-B solver with the multistart method and tested, as N is increased, for convergence of the bilayer energy in Eq. (4).

APPENDIX E: CALCULATION OF PROTEIN INTERACTION POTENTIALS IN HETEROGENEOUS BILAYERS

In this Appendix we elaborate on the method by which we obtain the protein interaction potentials $G_{\text{int}}(L)$ in Sec. IV

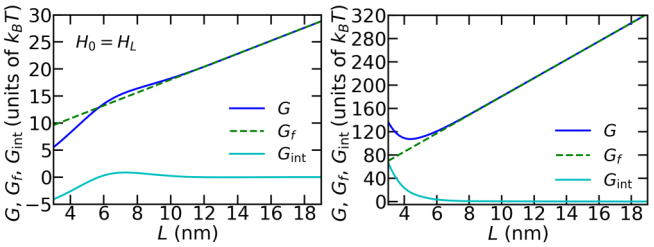

FIG. 14. Total bilayer energy G in Eq. (4), protein interaction potential in Eq. (E1) and far-field bilayer energy G_f in Eq. (E2) as a function of protein separation L for membrane proteins with identical hydrophobic thickness $H_0 = H_L = 2.0$ nm (left panel) and distinct hydrophobic thicknesses $H_0 = 2.2$ nm and $H_L = 1.3$ nm (right panel) in heterogeneous bilayers. For both panels we used natural boundary conditions on c at all bilayer-protein interfaces, and set $\mu = 0$ and $\tau = 0$.

for heterogeneous lipid bilayers (Figs. 7 and 8). To calculate $G_{\text{int}}(L)$, we subtract from the total bilayer energy G in Eq. (4) the value of G obtained in the large-L, noninteracting regime. With the mean-field model in Fig. 6, a complication arises here in that G tends to increase linearly with L as $L \to \infty$ (see Fig. 14) because, for large L, the bilayer energy associated with the bilayer-protein interactions at the outer membrane patch boundary is approximately proportional to the circumference of the outer membrane patch boundary. We thus set

$$G_{\text{int}}(L) = G(L) - G_f(L), \tag{E1}$$

where we take the far-field bilayer energy G_f to be of the form

$$G_f(L) = A\,L + B, \tag{E2}$$

where A and B are constants. Equation (E1) ensures that $G_{\text{int}}(L) \to 0$ as $L \to \infty$. For each $G_{\text{int}}(L)$ considered in Figs. 7 and 8, we determine the values of A and B by fitting Eq. (E2) to $G(L)$ in the range $15\ \text{nm} \leqslant L \leqslant 20$ nm, sampling $G(L)$ at increments of 0.5 nm. For instance, for $\mu = 0$ and $\tau = 0$, we have $A \approx 1.2\ k_BT/\text{nm}$ and $B \approx 6.0\ k_BT$ in Eq. (E2) for membrane proteins with natural boundary conditions on c and identical hydrophobic thickness $H_0 = H_L = 2.0$ nm (left panel in Fig. 14), while for membrane proteins with natural boundary conditions on c and distinct hydrophobic thicknesses $H_0 = 2.2$ nm and $H_L = 1.3$ nm we have $A \approx 15.8\ k_BT/\text{nm}$ and $B \approx 22.5\ k_BT$ in Eq. (E2) (right panel in Fig. 14). We do not subtract G_f from G for any calculations in the main text of this article other than those connected to Figs. 7 and 8. In particular, we consider the total bilayer energy G in Eq. (4) for the cooperative gating curves in Fig. 9.

[1] D. M. Engelman, Nature (London) **438**, 578 (2005).
[2] G. van Meer, D. R. Voelker, and G. W. Feigenson, Nat. Rev. Mol. Cell Biol. **9**, 112 (2008).
[3] E. Sezgin, I. Levental, S. Mayor, and C. Eggeling, Nat. Rev. Mol. Cell Biol. **18**, 361 (2017).
[4] K. Jacobson, O. G. Mouritsen, and R. G. W. Anderson, Nat. Cell Biol. **9**, 7 (2007).
[5] R. G. W. Anderson and K. Jacobson, Science **296**, 1821 (2002).
[6] T. Baumgart, A. T. Hammond, P. Sengupta, S. T. Hess, D. A. Holowka, B. A. Baird, and W. W. Webb, Proc. Natl. Acad. Sci. USA **104**, 3165 (2007).

[7] A. R. Honerkamp-Smith, S. L. Veatch, and S. L. Keller, Biochim. Biophys. Acta Biomembranes **1788**, 53 (2009).
[8] M. Rao and S. Mayor, Curr. Opin. Cell Biol. **29**, 126 (2014).
[9] A. Anishkin and C. Kung, Proc. Natl. Acad. Sci. USA **110**, 4886 (2013).
[10] D. Schmidt and R. MacKinnon, Proc. Natl. Acad. Sci. USA **105**, 19276 (2008).
[11] A. H. Beaven, A. M. Maer, A. J. Sodt, H. Rui, R. W. Pastor, O. S. Andersen, and W. Im, Biophys. J. **112**, 1185 (2017).
[12] W. Rawicz, K. Olbrich, T. McIntosh, D. Needham, and E. Evans, Biophys. J. **79**, 328 (2000).
[13] G. Chang, R. H. Spencer, A. T. Lee, M. T. Barclay, and D. C. Rees, Science **282**, 2220 (1998).
[14] E. Perozo, D. M. Cortes, P. Sompornpisut, A. Kloda, and B. Martinac, Nature (London) **418**, 942 (2002).
[15] H. W. Huang, Biophys. J. **50**, 1061 (1986).
[16] N. Dan, P. Pincus, and S. A. Safran, Langmuir **9**, 2768 (1993).
[17] O. S. Andersen and R. E. KoeppeII, Annu. Rev. Biophys. Biomol. Struct. **36**, 107 (2007).
[18] R. Phillips, T. Ursell, P. Wiggins, and P. Sens, Nature (London) **459**, 379 (2009).
[19] N. Mobashery, C. Nielsen, and O. S. Andersen, FEBS Lett. **412**, 15 (1997).
[20] C. Nielsen, M. Goulian, and O. S. Andersen, Biophys. J. **74**, 1966 (1998).
[21] E. Perozo, A. Kloda, D. M. Cortes, and B. Martinac, Nat. Struct. Biol. **9**, 696 (2002).
[22] P. Wiggins and R. Phillips, Proc. Natl. Acad. Sci. USA **101**, 4071 (2004).
[23] J. Yuan, F. Jin, T. Glatter, and V. Sourjik, Proc. Natl. Acad. Sci. USA **114**, E10792 (2017).
[24] N. Dan, A. Berman, P. Pincus, and S. A. Safran, J. Phys. II France **4**, 1713 (1994).
[25] T. Ursell, K. C. Huang, E. Peterson, and R. Phillips, PLoS Comp. Bio. **3**, e81 (2007).
[26] C. A. Haselwandter and R. Phillips, Europhys. Lett. **101**, 68002 (2013).
[27] O. Kahraman, W. S. Klug, and C. A. Haselwandter, Europhys. Lett. **107**, 48004 (2014).
[28] O. Kahraman, P. D. Koch, W. S. Klug, and C. A. Haselwandter, Phys. Rev. E **93**, 042410 (2016).
[29] T. A. Harroun, W. T. Heller, T. M. Weiss, L. Yang, and H. W. Huang, Biophys. J. **76**, 937 (1999).
[30] R. L. Goforth, A. K. Chi, D. V. Greathouse, L. L. Providence, R. E. KoeppeII, and O. S. Andersen, J. Gen. Physiol. **121**, 477 (2003).
[31] A. V. Botelho, T. Huber, T. P. Sakmar, and M. F. Brown, Biophys. J. **91**, 4464 (2006).
[32] S. L. Grage, A. M. Keleshian, T. Turdzeladze, A. R. Battle, W. C. Tay, R. P. May, S. A. Holt, S. A. Contera, M. Haertlein, M. Moulin, P. Pal, P. R. Rohde, T. V. Forsyth, A. Watts, K. C. Huang, A. S. Ulrich, and B. Martinac, Biophys. J. **100**, 1252 (2011).
[33] C. A. Haselwandter and N. S. Wingreen, PLoS Comput. Biol. **10**, e1003932 (2014).
[34] D. Milovanovic, A. Honigmann, S. Koike, F. Göttfert, G. Pähler, M. Junius, S. Müllar, U. Diederichsen, A. Janshoff, H. Grubmüller, H. J. Risselada, C. Eggeling, S. W. Hell, G. van den Bogaart, and R. Jahn, Nat. Commun. **6**, 5984 (2015).
[35] O. Kahraman, P. D. Koch, W. S. Klug, and C. A. Haselwandter, Sci. Rep. **6**, 19214 (2016).
[36] A. M. Pollard and V. Sourjik, J. Biol. Chem. **293**, 2149 (2018).
[37] C. A. Haselwandter and R. Phillips, PLoS Comput. Biol. **9**, e1003055 (2013).
[38] A. Shrestha, O. Kahraman, and C. A. Haselwandter, Phys. Rev. E **102**, 060401(R) (2020).
[39] E. Schäffer and U. Thiele, Eur. Phys. J. E **14**, 169 (2004).
[40] E. J. Wallace, N. M. Hooper, and P. D. Olmsted, Biophys. J. **90**, 4104 (2006).
[41] S. Leibler and D. Andelman, J. Phys. France **48**, 2013 (1987).
[42] P. Sens and S. Safran, Eur. Phys. J. E **1**, 237 (2000).
[43] S. A. Rautu, G. Rowlands, and M. S. Turner, Phys. Rev. Lett. **114**, 098101 (2015).
[44] P. Wiggins and R. Phillips, Biophys. J. **88**, 880 (2005).
[45] H.-G. Döbereiner, E. Evans, U. Seifert, and M. Wortis, Phys. Rev. Lett. **75**, 3360 (1995).
[46] P. B. Sunil Kumar, G. Gompper, and R. Lipowsky, Phys. Rev. E **60**, 4610 (1999).
[47] S. A. Safran, *Statistical Thermodynamics of Surfaces, Interfaces, and Membranes* (Westview, Boulder, 2003)
[48] S. L. Veatch and S. L. Keller, Phys. Rev. Lett. **89**, 268101 (2002).
[49] S. L. Veatch and S. L. Keller, Biophys. J. **85**, 3074 (2003).
[50] L. Foret, Europhys. Lett. **71**, 508 (2005).
[51] B. A. Camley and F. L. H. Brown, Phys. Rev. Lett. **105**, 148102 (2010).
[52] B. A. Camley and F. L. H. Brown, J. Chem. Phys. **135**, 225106 (2011).
[53] A. R. Honerkamp-Smith, B. B. Machta, and S. L. Keller, Phys. Rev. Lett. **108**, 265702 (2012).
[54] T. Ursell, J. Kondev, D. Reeves, P. A. Wiggins, and R. Phillips, in *Mechanosensitivity in Cells and Tissues 1: Mechanosensitive Ion Channels*, edited by A. Kamkin and I. Kiseleva (Springer, New York, 2008), pp. 37–70.
[55] H.-J. Kaiser, A. Orłowski, T. Róg, T. K. M. Nyholm, W. Chai, T. Feizi, D. Lingwood, I. Vattulainen, and K. Simons, Proc. Natl. Acad. Sci. USA **108**, 16628 (2011).
[56] B. B. Diaz-Rohrer, K. R. Levental, K. Simons, and I. Levental, Proc. Natl. Acad. Sci. USA **111**, 8500 (2014).
[57] J. T. Marinko, A. K. Kenworthy, and C. R. Sanders, Proc. Natl. Acad. Sci. USA **117**, 14168 (2020).
[58] A. M. Powl, J. M. East, and A. G. Lee, Biochemistry **42**, 14306 (2003).
[59] A. M. Powl, J. M. East, and A. G. Lee, Biochemistry **47**, 12175 (2008).
[60] Y. A. Ermakov, K. Kamaraju, K. Sengupta, and S. Sukharev, Biophys. J. **98**, 1018 (2010).
[61] A. Laganowsky, E. Reading, T. M. Allison, M. B. Ulmschneider, M. T. Degiacomi, A. J. Baldwin, and C. V. Robinson, Nature (London) **510**, 172 (2014).
[62] T. Harayama and H. Riezman, Nat. Rev. Mol. Cell Biol. **19**, 281 (2018).
[63] V. Corradi, B. I. Sejdiu, H. Mesa-Galloso, H. Abdizadeh, S. Y. Noskov, S. J. Marrink, and D. P. Tieleman, Chem. Rev. **119**, 5775 (2019).
[64] S. Schrecke, Y. Zhu, J. W. McCabe, M. Bartz, C. Packianathan, M. Zhao, M. Zhou, D. Russell, and A. Laganowsky, Nat. Chem. Biol. **17**, 89 (2021).

[65] M. T. Agasid and C. V. Robinson, Curr. Opin. Struct. Biol. **69**, 78 (2021).
[66] Y. R. Guo and R. MacKinnon, eLife **6**, e33660 (2017).
[67] C. A. Haselwandter and R. MacKinnon, eLife **7**, e41968 (2018).
[68] Y.-C. Lin, Y. R. Guo, A. Miyagi, J. Levring, R. MacKinnon, and S. Scheuring, Nature (London) **573**, 230 (2019).
[69] D. Argudo, N. P. Bethel, F. V. Marcoline, C. W. Wolgemuth, and M. Grabe, Biophys. J. **112**, 2159 (2017).
[70] J. B. Fournier, Eur. Phys. J. B **11**, 261 (1999).
[71] A. J. Bray, Adv. Phys. **51**, 481 (2002).
[72] T. Baumgart, S. T. Hess, and W. W. Webb, Nature (London) **425**, 821 (2003).
[73] R. H. Byrd, P. Lu, J. Nocedal, and C. Zhu, SIAM J. Sci. Comput. **16**, 1190 (1995).
[74] C. Zhu, R. H. Byrd, P. Lu, and J. Nocedal, ACM Trans. Math. Softw. **23**, 550 (1997).
[75] R. Courant and D. Hilbert, *Methods of Mathematical Physics* (Interscience Publishers, New York, 1953).
[76] B. van Brunt, *The Calculus of Variations* (Springer, New York, 2004).
[77] C.-S. Chiang, A. Anishkin, and S. Sukharev, Biophys. J. **86**, 2846 (2004).
[78] T. Auth and G. Gompper, Phys. Rev. E **80**, 031901 (2009).
[79] M. M. Müller and M. Deserno, Prog. Theor. Phys. Suppl. **184**, 351 (2010).
[80] D. Li, O. Kahraman, and C. A. Haselwandter, Phys. Rev. Lett. **117**, 138103 (2016).
[81] E. Zauderer, *Partial Differential Equations of Applied Mathematics* (Wiley, New York, 1983).
[82] *Mathematica 12.1.1* (Wolfram Research, Inc., Champaign, IL 2020).
[83] Z. Wu, *Lecture Notes on Computational Structural Biology* (World Scientific, Singapore, 2008).
[84] R. Martí, J. A. Lozano, A. Mendiburu, and L. Hernando, *Handbook of Heuristics* (Springer, Cham, 2018).